Check for updates

Evaluation of historical CMIP6 model simulations and future climate change projections in the Baro River Basin

Bekele Terefe Gebisa[a], Wakjira Takala Dibaba [ID][b,]* and Alemayehu Kabeta[a]

[a] Department of Hydraulic and Water Resources Engineering, Bule Hora University, Bule Hora, Ethiopia
[b] Department of Hydraulic and Water Resources Engineering, Jimma University, Jimma, Ethiopia
*Corresponding author. E-mail: wak.nimona@gmail.com

[ID] WTD, 0000-0002-9359-2142

ABSTRACT

This study evaluated the performance of five Global Climate Model (GCM) outputs from the Coupled Model Intercomparison Project phase 6 (CMIP6) in reproducing the historical precipitation and temperature. Observational data from the National Meteorological Agency are used for model evaluation and bias correction. Then, the projections from representative GCMs are used to understand the future climate (2031–2060) of the Baro River Basin under two Shared Socioeconomic Pathways (SSP2-4.5 and SSP5-8.5) with respect to the historical datasets (1985–2014). Statistical metrics (percent of bias, root mean square error, and coefficient of determination) are used to assess the model's performance in reproducing precipitation and temperature and Compromise Programming (CP) was used in ranking GCMs. GFDL-CM4, INM-CM5-0, and INM-CM4-8 models for precipitation; CMCC-ESM2, MRI-ESM2-0, and INM-CM4-8 for maximum temperature; and GFDL-CM4, INM-CM4-8, and INM-CM5-0 for minimum temperature were selected based on their better simulation. The projected annual precipitation shows increases of 6% under SSP2-4.5 and 16.46% under SSP5-8.5. The mean annual maximum and minimum temperature show increases of 1.43 and 1.96 °C under SSP2-4.5, and 1.81 and 3.11 °C under SSP5-8.5, respectively. Overall, the ensemble of three models outperforms the ensemble of all models for the Baro River Basin when utilising the representative GCMs.

Key words: Baro River, climate projection, CMIP6, GCMs, performance

HIGHLIGHTS

- Multi-model GCM outputs help in reducing model discrepancies.
- Multi-criteria evaluation enables the development of proactive approach to facilitate evaluation.
- Relying solely on the ensemble of all models is not suitable for climate impact studies.
- Careful model selection in climate impact studies should be emphasized.
- Comprehensive understanding of climate dynamics helps to explore the future outlook of regions.
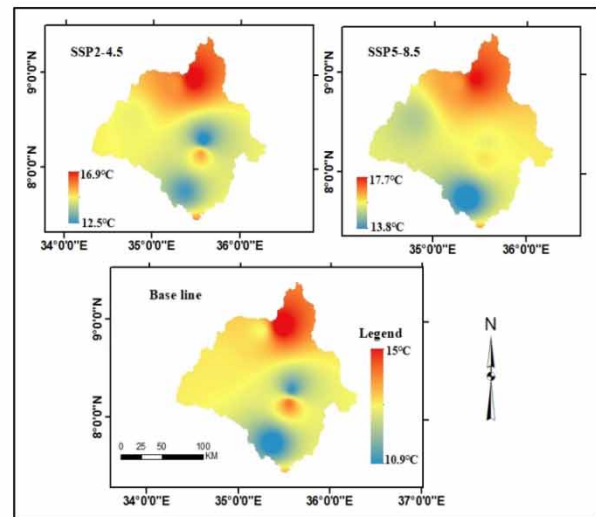
GRAPHICAL ABSTRACT

Spatial distribution of annual precipitation (2031-2060)
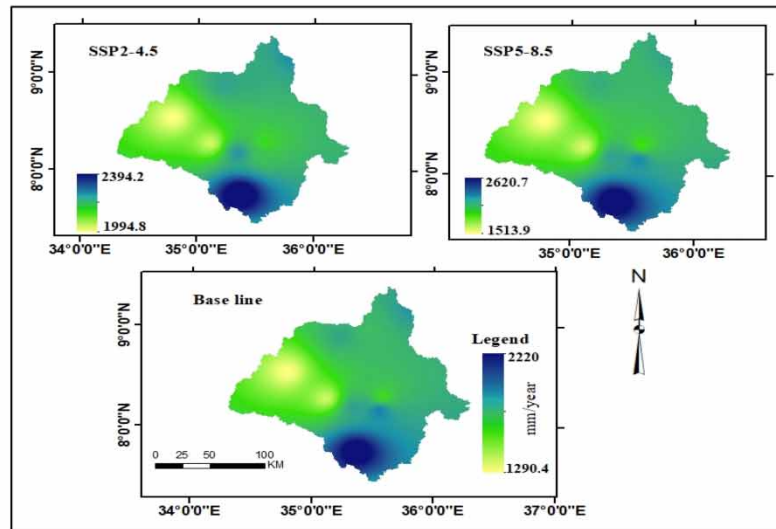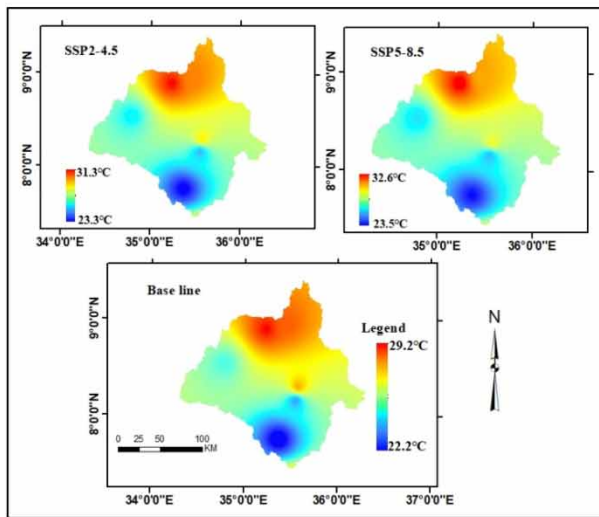
Spatial distribution of maximum temperature (2031-2060)　　　Spatial distribution of minimum temperature (2031-2060)

1. INTRODUCTION

Rapid global warming has hastened global and regional climate change, changing the severity and frequency of extreme climatic events with far-reaching consequences on natural ecosystems, human development and significant economic losses each year (Chen *et al.* 2020; Srivastava *et al.* 2020; Ge *et al.* 2021; Wu *et al.* 2021). Understanding the intensity, frequency, and spatial extents through reliable future projections of climate changes is a pre-requisite to make reliable climate change adaptation planning (Kim *et al.* 2020). Due to its low adaptability and resilience to natural disasters, climate changes have serious implications for developing countries such as Africa. Moreover, weak adaptive capacity due to limited access to information, technology, finance, and capital assets, intensifies the impacts of climate change in developing countries (Sylla *et al.* 2016). According to IPCC (2013), in many parts of Africa, changes in rainfall and temperature are causing fluctuations in freshwater systems, affecting the quality and quantity of water accessibility.

Ethiopia relies primarily on available water resources from the highlands and rain-fed agriculture, but much of the south and east region is very dry and prone to drought and desertification (Roth *et al.* 2018). Over the past 55 years, it has been

known that there was a warming trend in the annual minimum temperature ranges, increasing by about 0.37 °C every decade (NMA 2007). The climate changes studies in different parts of Ethiopia revealed that climate change-induced changes in seasonal and annual hydrological variables show increasing stress on water resources availability (Melke 2015; Shiferaw *et al.* 2018; Taye *et al.* 2018; Worku *et al.* 2018; Dibaba *et al.* 2020; Mengistu *et al.* 2020). However, different studies reported varying magnitudes of the impacts. For example, Mengistu *et al.* (2020) and Dibaba *et al.* (2020) reported increasing mean annual temperature and decreasing precipitation in the Upper Blue Nile river basin and Finchaa catchment, respectively. Temperature increases have also been reported in the Ilala watershed, but there has been no significant change in precipitation (Shiferaw *et al.* 2018). According to Melke (2015), the monthly and seasonal temperature and precipitation in the future time horizons did not show a systematic increase or decrease in Gumara Catchment, Lake Tana Basin.

Despite being the main water resource for Nile basin riparian countries, the Baro River Basin is facing immense pressure and different competitive uses. Moreover, the Baro River Basin is subject to high climate variability with frequent changes in hydrology as a result of climate change (Mengistu *et al.* 2021; Muleta 2021). Variations in the hydrological process due to climate change-induced extreme events and water scarcity limits agricultural production and the community livelihood in the basin and the country at large. For example, using the A1B emission scenario, Muleta (2021) reported an increase in temperature, but precipitation does not manifest a systematic increase or decrease. Mengistu *et al.* (2021) reported increasing temperature and decreasing annual precipitation trends for the same basin using bias-corrected CORDEX-RCMs (Regional Climate Models). Overall, climate projections indicated that current water stress challenges will be exacerbated under a warming climate. All scenarios projected warmer temperature, but the studies have shown discrepancies in precipitation predictions. This could be due to the nature of precipitation, type of climate models and characteristics of climate scenarios adopted. One mechanism for reducing climate model discrepancies is the use of multi-model GCMs (Dibaba *et al.* 2019). However, using multi-model GCMs requires a proper evaluation of the model's performance before identifying representative GCMs for a particular location (Kim *et al.* 2020). It is therefore critical to assess, identify and map the long-term climate projections using state-of-the-art climate modeling with the latest datasets to aid the development of water resources in the basin.

Projections of global climate variables have been carried out using General Circulation Models, which provide projections at large spatial scales. Jaagus & Mändla (2014) stated that greenhouse gas concentrations are used as input statistics for the GCM. Over the years, many of the GCMs have been developed for various IPCC assessment report scenarios, including phases 3 and 5 of the Coupled Model Intercomparison Project (CMIP) and the recently released phase 6. The main differences between the CMIP6 simulations and the previous CMIP phases (CMIP3 and CMIP5) are the future scenario start years and new sets of specifications for concentration, emission, and land-use scenarios (Gidden *et al.* 2019). Moreover, CMIP6 represents a major increase in terms of the number of modeling groups involved, the number of future scenarios considered, and the number of diverse experiments conducted (Chen *et al.* 2020). From GCMs to Earth System Models, CMIP6 models have a wider range of complexity due to improved physical processes and higher spatial resolution (Eyring *et al.* 2016). The Scenario Model Intercomparison Project (Scenario MIP) is the primary activity of CMIP6 and is based on alternative scenarios of future emissions and land-use change generated by integrated assessment models.

Climate change projections are critical for improving the understanding of the climate system as well as characterizing societal risks and response options (O'Neill *et al.* 2016). To explore the impacts of climate change, adaptation, and mitigation, CMIP6 utilizes a new scenario framework combining future radiative forcing and associated climate changes with alternative socioeconomic development pathways (SSPs) (O'Neill *et al.* 2014). In conclusion, CMIP6 is preferred over CMIP5 due to a number of characteristics that improve climate projections. A wide range of enhancements provided by CMIP6 includes increased resolution, broader parameterization, and updated emission scenarios. These advancements considerably bolster the precision and comprehensiveness of climate forecasting. Moreover, CMIP6 incorporated the most recent generation of climate models, integrating the latest insights into climate processes and featuring improved representations of physical, chemical, and biological interactions. Additionally, CMIP6 introduces a broader spectrum of Earth system components model processes, including land-use changes, biogeochemical cycles, and ice-sheet dynamics. The incorporation of these novel elements amplifies the models' capacity to capture intricate interactions and feedback mechanisms within the Earth system. Consequently, the projections generated by CMIP6 encompass a more comprehensive understanding of the complex dynamics governing our planet.

A number of studies have evaluated the performance of CMIP6 climate model outputs using GCM simulations (eg. Karim *et al.* 2020; Afolayan *et al.* 2021; Babaousmail *et al.* 2021; Ngoma *et al.* 2021; Shiru & Chung 2021; Zhang *et al.* 2021; Zhou *et al.* 2021). However, being recently released, CMIP6 is not known to have been applied in the Baro River Basin. On the

other hand, there have only been a few studies on climate projection in the Baro River Basin and the analysis of previous studies was not based on recent climate model projections. Some of the climate change studies in the basin were projected based on climate scenarios A1B (balanced scenario group of storyline A1) and B1 (intermediate level of the storyline) (Kebede *et al.* 2013; Muleta 2021). Although increasing temperature is reported by the studies, the studies have shown discrepancies in precipitation predictions. In the previous climate scenarios, describing the developments of anthropogenic drivers for the possible future climate change with socioeconomic development is inattentive. The studies are also based on the application of a single climate model without any performance evaluation among the alternative climate models. It is true that most of the climate change studies in Ethiopia are based on either a single GCM–RCM model or do not involve model evaluations before using GCM–RCM for climate change and impact assessments as also used in the Baro Akobo River basin. We believe that one mechanism for reducing climate model discrepancies is the use of multi-model GCMs with the most recent state-of-the-art climate models available using proper evaluation of the individual and ensemble models. However, using multi-model GCMs requires a proper evaluation of the model's performance before identifying representative GCMs for a particular location. In this regard, comprehensive investigation is required to establish the improvements of CMIP6 models in simulating precipitation and temperature over various spatio-temporal scales and the selection of climate models for climate projections and impact studies requires assessment of multi-model performance.

The new approach used in this study, the use of multi-model output using multi-criteria evaluation, has a very important contribution for proper establishment of comprehensive assessments of multiple GCMs under various scenarios in Ethiopia where only limited information is available to develop proper strategic information in understanding current and future climate projections for a better adaptive capacity and mitigations. The contribution could also be related to evaluating the models' dependability, understanding their strengths and limitations, or identifying the most appropriate model for a specific application. The new set of simulations will also help to evaluate key aspects of society with a comprehensive potential climates that would imply a range of challenges in mitigating and adapting to climate change and socioeconomic outcomes. Consequently, this research emphasized on developing a more comprehensive understanding of the regional climate governing the region through careful model selection and evaluation which also help to explore the future outlook of the basin.

Based on the five GCMs obtained from the CMIP6 model, the objectives of the current study were to: (a) evaluate the capability of the CMIP Phase 6 (CMIP6) based Global Climate Models (GCMs) to accurately simulate precipitation, maximum temperature, and minimum temperature in the Baro River Basin; (b) evaluate the effectiveness of bias-corrected GCM simulations in replicating observed precipitation, as well as maximum and minimum temperature patterns; (c) quantify the projected alterations in future precipitation, maximum temperature, and minimum temperature.

2. MATERIALS AND METHODS

2.1. Study area

The Baro River is a transboundary river that originates from the western highlands of Ethiopia and flows into the Nile River (Mengistu *et al.* 2021). Geographically, it is found between latitudes 5°40′ and 10°50′ N and longitude 33°20′ and 36°20′ E. in west Ethiopia (Figure 1). The river basin has a complex topography with an elevation ranging from a minimum elevation of 416 m and a maximum of 3,266 m. Owing to the large differences in elevation within the basin, the area is characterized by different climatic conditions.

The basin is bordered by Sudan to the west, the Upper Blue Nile basin to the north and northeast, and the Akobo River to the east and southeast. The Baro River is formed by the confluence of the Birbir and Gebba Rivers east of Metu in the Illuababor zone of the Oromia region. The study area is covered 23,500 km^2 with the outlet at the Gambella station. Mean monthly precipitation in the basin varies from about 23 mm in February to more than 300 mm in August, with two distinct seasons. From April to October is the rainy season, and from November to March is the dry season. The average monthly maximum temperature ranges from 23 °C in July to 30 °C in March, while the minimum temperature in the basin ranges from 12 °C in June to 14 °C in January

2.2. Datasets

2.2.1. Observed data

Daily meteorological data were collected from National Meteorological Agency (NMA) and used to evaluate the GCMs model output data before using the GCMs simulations for future projection of climate change. For undertaking climate analysis, complete datasets with no gaps or missing information are typically required (Dibaba *et al.* 2019). In this respect, rainfall
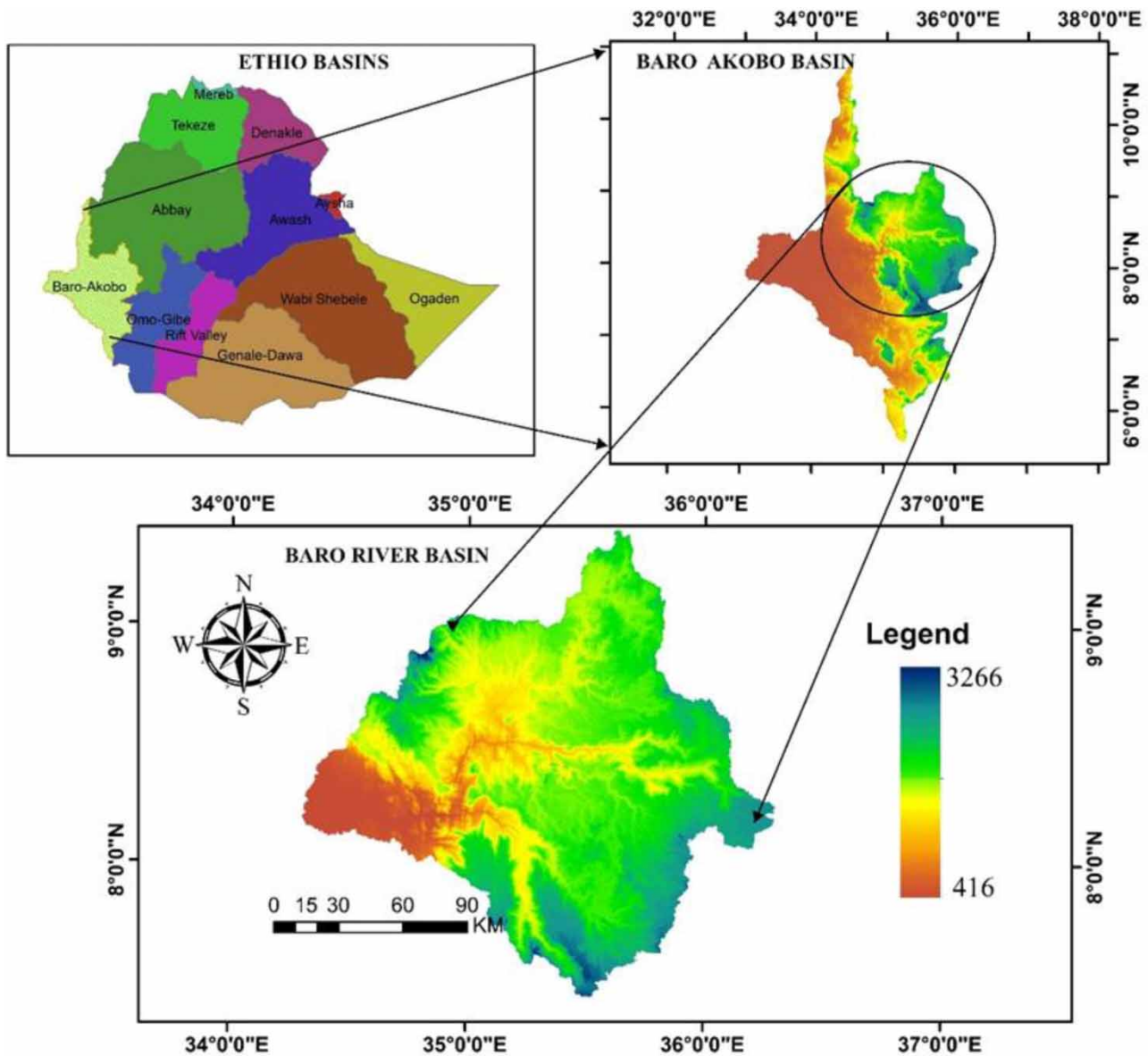
Figure 1 | Location map of the Baro River Basin.

stations with a significant number of missing values are excluded from the evaluation process. Eleven stations were chosen for precipitation data, while seven stations were selected for maximum and minimum temperature, as indicated in Table 1. In both cases, all the selected stations have missing values of less than 10% for the records. In this research, the missing meteorological data were filled with the Markov Chain Monte Carlo (MCMC) imputation technique using XLSTAT. The quality and consistency of the meteorological data were checked using the homogeneity test and Double Mass Curve analysis.

2.2.2. CMIP6 Global Climate Model (GCM) data

In this study, the CMIP6 GCMs were used to simulate precipitation and temperature in the Baro River Basin. A set of criteria was used to select among the various GCMs from the CMIP6. They include: the nominal resolution (100 km), scenario/experiment and analysis period. Further, the availability of the CMIP6 models with a complete first ensemble member (r1i1p1f1) at the time of analysis was considered, i.e. only models having a similar variant label are used in order to have an unbiased comparison of all of them. In this case, models with different variant labels are not considered

Table 1 | Observed point data information used in this study

No.	Name of stations	Latitude	Longitude	Elevation	Tmax	Tmin	PCP
1	Aemteferi	8.9	35.23333	1,630	✓	✓	✓
2	Bure	8.28	35.11	1,704			✓
3	Gimbi	9.201389	35.83944	1,844			✓
4	Gore	8.157283	35.54983	2,024	✓	✓	✓
5	Masha	7.752683	35.37	2,235	✓	✓	✓
6	Mizenteferi	7.0026	35.58428	1,444			✓
7	Matuhospital	8.297067	35.57615	1,702	✓	✓	✓
8	Tepi	7.204883	35.43748	1,208	✓	✓	✓
9	Uka	8.18	35.35	1,667			✓
10	Yubdo	8.9525	35.44694	1,550	✓	✓	✓
11	Dembidollo	8.54	34.79	1,811	✓	✓	✓

Note: ✓ represents the data are available at that station, PCP means precipitation, T_{max} means maximum temperature and T_{min} means the minimum temperature of the observed data.

for comparisons as models with different variant labels can be associated to different realization, initialization and characteristics. Moreover, only models that have three simulation conditions, i.e. historical simulations, and SSP2-4.5 and SSP2-4.5 simulations for both precipitation and temperature are only considered. Considering these factors five GCMs are selected (Table 2). Historical data from 1985 to 2014 was used as a baseline for this study. Future climate datasets from CMIP6 GCMs are available from 2015 to 2100. For each model, precipitation, maximum, and minimum temperature data are obtained for the SSP2-4.5 and SSP5-8.5 scenarios. Further information on the GCMs data used is available online at (https://esgf-node.IInI.gov/search/cmip6/).

2.3. Methods

2.3.1. Global climate models performance evaluation

The performance of the five CMIP6 models in simulating the climate of the Baro River Basin was evaluated using historical simulations of the model with observed data. For comparison, all datasets were re-gridded to the same resolution using Climate Data Operator (CDO). The Max Planck Institute for Meteorology has developed the CDO, which is a collection of statistical and mathematical commands for processing atmospheric data in GRIB and NetCDF formats. CDO contains a number of operators that are used to consistently analyze climate and forecast model data. A Cygwin package was used to execute the commands for this paper. Interpolation was performed using the bilinear interpolation method to allow evaluations at the same resolution and to extract the data at the required latitude and longitude (Figure 2).

Inverse distance weighting (IDW) calculates values for unsampled points using a weighted average of the observed data at nearby locations (Dibaba *et al.* 2019). This implies that values at unsampled locations can be estimated using a linear combination of values at known sampled points. IDW is based on the idea that closer points have a greater influence on the

Table 2 | Basic information on the CMIP6 used in this study

| Model name	Institution and country	Resolution (Lon × Lat)	Variant label
CMCC-ESM2	Fondazione Centro Euro-Mediterraneo sui Cambiamenti Climatici, Italy	1.25° × 0.9424°	r1i1p1f1
GFDL-CM4	Geophysical Fluid Dynamics Laboratory, Princeton, USA	1.25° × 1°	r1i1p1f1
INM-CM4-8	Institute for Numerical Mathematics, Russia	2° × 1.5°	r1i1p1f1
INM-CM5-0	Institute for Numerical Mathematics, Russia	2 × 1.5	r1i1p1f1
MRI-ESM2-0	Meteorological Research Institute, Japan	1.125° × 0.9424°	r1i1p1f1
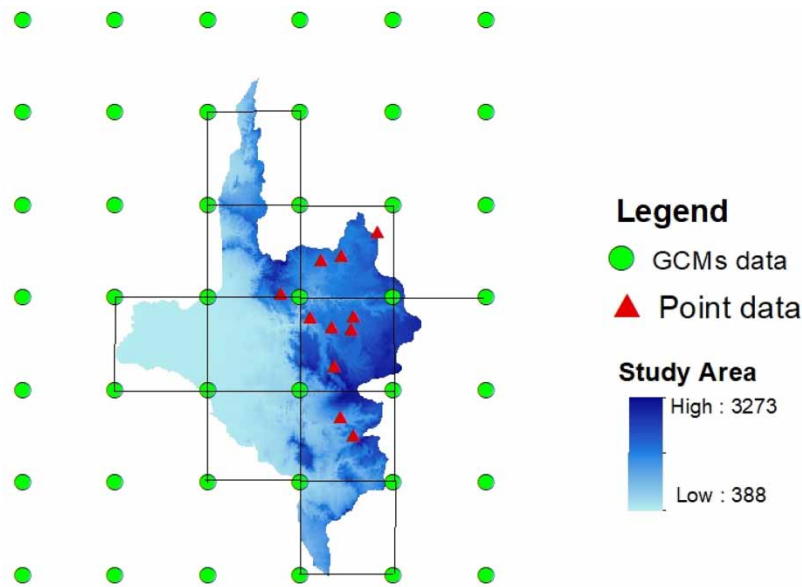
Figure 2 | The gridded GCM data and point data in the study area.

unknown value of a point than distance points. Weighted value can be determined using Equation (1):

$$Ws = \frac{\sum\limits_{i}^{n} 1/di2wi}{\sum\limits_{i}^{n} 1/di2} \tag{1}$$

where Ws is the interpolated value at the considered station, wi is the data at grid point i, di is the distance from grid point, i to the station, and n is the total number of grid points surrounding the stations.

To evaluate the model performance, statistical data analysis such as root mean square error (RMSE), percentage of bias (PBIAS), and coefficient of determination (R^2) were used (Karim *et al.* 2020; Babaousmail *et al.* 2021; Shiru & Chung 2021). The empirical formulas used to compute the performance evaluation are given in Equations (2)–(4). PBIAS indicates how close the mean of GCMs is to the mean observed value. A bias ratio closer to 0 indicates that GCMs rainfall estimate data is closer to observation data and is considered an ideal score:

$$\text{PBIAS} = \frac{1}{n} \sum_{i=i}^{n} (S_i - O_i) * 100 \tag{2}$$

$$R^2 = \frac{\sum\limits_{i=1}^{n} [(O_i - O_m)(S_i - S_m)]^2}{\sum\limits_{i=1}^{n} \left[(O_i - O_m)^2 \sum\limits_{i=0}^{n} (S_i - S_m)^2 \right]} \tag{3}$$

$$\text{RMSE} = \sqrt{\frac{1}{n} \sum_{i=1}^{n} (S_i - O_m)^2} \tag{4}$$

where S is the simulated value of the GCMs and O is the observed value of the climate variable, i refers to the simulated and observed pairs, n is the total number of the pairs, and m refers to mean. RMSE measures the difference between GCMs and observed data. An RMSE value close to zero indicates better performance. It states how concentrated the data is around the line of best fit; a measure of 0 is the optimal score. The coefficient of determination (R^2) quantifies the correlation between the

CMIP6 models and observations, with a value closer to 0 indicating no correlation and a value closer to 1 indicating perfect correlation.

2.3.2. Compromise programming

Compromise programming (CP) is a method for calculating the combined effect of various statistical indices (Zeleny 1973; Shiru & Chung 2021). In this study, CP was used to rank GCMs based on the three statistical indices: RMSE, PBIAS, and R^2. The statistical indices values were used to estimate the CP distance measure (Lp) metric where Lp metric can be expressed using Equation (5) (Shiru & Chung 2021):

$$Lp = \left[\sum_{j=1}^{3} (f\_j^* - f\_j)p \right]^{1/p} \tag{5}$$

where $f\__j$ is the normalized value of the statistical performance measure j, $f\__j^*$ is the normalized ideal value of the statistical performance measure j, and p is a parameter which is equal to 1. The ideal value for a statistical performance measure is the one that corresponds to a perfect match between relevant observations and model simulations. The Lp metric's value is always positive, and the lower the value, the better the model's performance; thus, the smallest values of Lp are preferred. For $p = 1$, all deviations from the maximum value f_j^* to the observed value of objective i are given equal importance. This indicates that decision makers have a low level of risk. Further details of the method can be found in Perez-Verdin et al. (2018), Muhammad et al. (2019) and Shiru & Chung (2021). According to Anil et al. (2021), normalizing the criteria before calculating the Lp metric value is crucial when using CP to rank GCMs. This is necessary to ensure that the criteria which may have varying ranges are transformed into a uniform range. In order to adjust these we considered the weight parameter of the CP method proposed by Raju & Kumar (2020) and Anil et al. (2021). Zhu et al. (2020) stated that the entropy weight method is frequently utilized as a weighting technique in decision-making to evaluate the dispersion of values. Moreover, Anil et al. (2021) noted that in the context of probability theory, increased entropy indicates decreased information quantity and greater uncertainty. Equations (6)–(8) are used to calculate the weights for each criterion (Zhu et al. 2020):

$$Ej = -\frac{1}{\ln M} \sum_{j=1}^{M} N\_ij \, \ln(N\_ij) \tag{6}$$

$$dj = 1 - Ej \tag{7}$$

$$wj = \frac{dj}{\sum_{j=1}^{n} dj} \tag{8}$$

where wj, Ej, and dj are weight, entropy and divergence of jth indicator, respectively. M is the total number of GCMs. After calculating performance metrics, we normalized the matrix element by using the method proposed by (Anil et al. 2021). Here, N_ij and J are normalized elements of the matrix and the total number of criteria in the matrix, respectively.

2.3.3. Downscaling

Downscaling is a method for producing high-resolution climate projections from coarse-resolution global climate models. While downscaling can provide more detailed information on climate variability and change, it also introduces additional uncertainties that must be taken into account. Some of the uncertainties associated with downscaling include model uncertainty, spatial and temporal uncertainty, and statistical uncertainty. The uncertainties associated with downscaling arise from the inherent uncertainty in the structure of downscaling models and the uncertainty in the input data (Khan et al. 2006). Downscaling often involves the use of statistical models to relate large-scale climate variables to local-scale variables. The accuracy of these statistical models depends on the availability and quality of data, assumptions made in the model, and other factors that can lead to statistical uncertainties. Despite these uncertainties, downscaling can be a useful tool for studying the regional or local effects of climate change. Downscaling can provide useful information for decision-making and planning, such as identifying areas that are particularly vulnerable to the effects of climate change or assessing the

effectiveness of various adaptation strategies. There are different techniques of downscaling the GCMs for climate change studies. For example, a recent study by Kadkhodazadeh *et al.* (2022) used a delta change factor for downscaling the CMIP6 GCMs and Kumar *et al.* (2023) used Empirical Quantile Mapping (EQM) to get the statistically downscaled and bias-corrected precipitation and temperature data. Both studies reported that downscaled GCMs products are more representative than the coarser GCMs. However, it is critical to recognize the limitations and uncertainties of downscaling and use the results appropriately. Overall, statistical and dynamical downscaling are the two main methods of interpolating GCM data (Flint & Flint 2012). The GCM results are utilized as boundary conditions for the regional-scale GCM models at finer-resolution when dynamically downscaling. This method requires sophisticated computers, and finer-scale, complete physical weather and ocean models, which are computationally costly. Statistical downscaling approaches use a statistical relationship between coarse and fine resolution historical climate records to interpolate from coarse model outputs to finer-resolution (Flint & Flint 2012). This requires less computational effort, but it frequently requires drastic simplifications of physical relationships. Statistical downscaling uses the application of different statistics-based approaches to discover links between large-scale climate patterns determined by global climate models and observable local climatic responses (Salihu 2018). These connections are used with GCM data to convert climate model outputs into statistically refined products that are frequently more suitable for use as input to regional or local climate impact studies. Owing to the above-mentioned facts, a statistical downscaling method was used in this study.

2.3.4. Bias correction

Many climate models and bias reduction methods recommend adopting an ensemble approach using bias-corrected data. The main idea is to parameterize the strain correction algorithms used to modify the simulated historical climate data with the observed historical climate variables and the simulated historical climate variables. The same correction algorithm applies to future climate data. Bias correction methods are used to minimize deviations between observed and simulated climate variables at daily time intervals, so hydrological simulations driven based on corrected simulated climate data are reasonably consistent with simulations using the observed climate data (Rathjens *et al.* 2016). There are different techniques of bias correction for precipitation and temperature. A recent study by Tumsa (2022) evaluated six bias correction techniques in the upper Awash basin of Ethiopia based on frequency and time series metrics. The result revealed Linear Scaling (LS) performed best in removing the model biases for precipitation. Dibaba *et al.* (2020) on the other hand reported Distribution Mapping (DM) as the best method in removing temperature biases. Furthermore, a thorough analysis of the bias correction techniques published by Teutschbein & Seibert (2012) revealed that each method has improved the simulation of precipitation and temperature biases. The percentiles and standard deviations of the daily precipitation series, however, fluctuate depending on the correction techniques used. Luo *et al.* (2018) also used five and seven bias correction methods for temperature and precipitation, respectively. The outcome showed that DM is able to minimize temperature biases while LS do for precipitation.

The LS method adjusts GCM/RCM simulation rainfall and temperature using multiplicative and additive factors, respectively (Worku *et al.* 2019). The factors are created by comparing observed data to historical GCM/RCM simulations. Using monthly adjustment values based on the variations between observed and raw data, it functions (raw GCMs simulated data in this case). Every month, precipitation is often multiplied to adjust for errors. The distribution function (CDF) of GCM-simulated rainfall and temperature values is adjusted with the CDF of observed rainfall and temperature values in the DM method. The DM method modifies the mean, standard deviation, extremes, and distribution of GCM/RCM output rainfall and temperature events. The Gamma and Gaussian distributions are used in DM to fit GCM/RCM rainfall and temperature distributions to observational data. For temperature, the Gaussian distribution (normal distribution) with a mean μ and a standard deviation is σ is usually assumed to fit temperature best.

This study used LS and DM methods to process the precipitation and temperature bias corrections, respectively. These bias correction techniques were selected owing to their effectiveness demonstrated in previous studies (Fang *et al.* 2015; Mengistu *et al.* 2021). Mengistu *et al.* (2021) in the Baro Akobo basin reported that LS performs slightly better than DM in correcting the bias from the individual raw models and ensemble for precipitation and DM outperforms LS for temperature bias correction.

2.3.5. Quantification of changes in precipitation and temperature

For future climate projection, a 30 year mean annual and monthly precipitation, maximum and minimum temperature data were analyzed for the baseline (1985–2014) and the near future (2031–2060). Precipitation and temperature scenarios

changed from daily totals to monthly and annual totals. Annual precipitation and temperature changes are calculated as differences and expressed as percentages. The changes in precipitation and temperature for the midterm projection with respect to the baseline are calculated using Equations (9) and (10) (Bodian *et al.* 2018):

$$\Delta T = \bar{T}GCMfut - \bar{T}GCMref \qquad (9)$$

$$\Delta P = \frac{(\bar{P}GCMfut - \bar{P}GCMref)}{\bar{P}GCMfut} * 100 \qquad (10)$$

where ΔT and ΔP are climate change scenarios of temperature and precipitation, respectively. $\bar{T}GCMfut$ and $\bar{P}GCMfut$ are the long-term average temperature and precipitation, respectively, simulated by the GCMs in the future period and $\bar{T}GCMref$ and $\bar{P}GCMref$ are long-term average temperature and precipitation, respectively, simulated by the model in a period similar to the observation data or baseline.

3. RESULTS AND DISCUSSIONS

3.1. Performance of GCM for precipitation

The calculated precipitation performance metrics for precipitation for all GCMs and the ranking of the GCMs derived using CP are shown in Table 3. The ideal values vary for each criterion, but the overall ranking indicates that the GCM that may have the most ideal values for more metrics does not necessarily rank best. For example, the ideal values of the percent of bias are 0.6 but the INM-CM5-0 is on the second rank. For precipitation, the top three GCMs are GFDL-CM4, INM-CM5-0, and INM-CM4-8, respectively. The lowest performing GCM for precipitation is CMCC-ESM2. For precipitation, the entropy method assigns weights of 0.27, 0.66, and 0.064 to the individual criteria RMSE, PBIAS, and R^2, respectively.

The difference between the matrix and the ideal value represents the statistical value, and the sum of all values represents the rank of the model, with lower values representing better performance and higher values representing the least performance. The percentage bias of the top three models is less than 7% and the R^2 value is greater than 0.855. Additionally, the three models follow unimodal rainfall. Therefore, based on observational data and comparing with historical GCM runs, the three climate models, i.e. GFDL-CM4, INM-CM5-0, and INM-CM4-8, are selected for precipitation.

Furthermore, the GCMs were evaluated using a 30 year mean annual precipitation. The 30-year areal-average of annual precipitation in the basin is 1,721.81 mm. The simulated mean annual precipitation is slightly underestimated and overestimated by GCMs. All models except GFDL-CM4 overestimated precipitation. GFDL-CM4 simulated annual precipitation of 1,626.65 mm whereas INM-CM5-0, INM-CM4-8, MRI-ESM2-0, and CMCC-ESM2 simulated mean annual rainfall as 1,732.15, 1,835.14, 1,966.45 and 2,283.84 mm, respectively. The spatial distribution of the historical (1985–2014) mean annual precipitation for the Baro River is shown in Figure 3. All GCMs except MRI-ESM2-0 and CMCC-ESM2 underestimated precipitation in the northern part of the basin. Mean annual precipitation around the western or outlet of the basin, eastern and central parts of the basin is overestimated by all GCMs. INM-CM4-8 and INM-CM5-0 simulated the observed precipitation whereas the other GCMs underestimated around the southern part. All models including the ensemble of the three models underestimated the northern and southern precipitation. However, the overall linear distribution over the

Table 3 | GCM performance metrics and ranking for precipitation

| GCM | Performance matrix | | | Normalized matrix | | | Normalized weighted matrix | | | | |
	RMSE	PBIAS	R^2	RMSE	PBIAS	R^2	RMSE	PBIAS	R^2	Sum	Rank
GFDL-CM4	15.71	−5.53	0.99	0.06	0.09	0.26	0.00	0.03	0.00	0.03	1
INM-CM4-8	39.25	6.58	0.86	0.16	0.11	0.22	0.03	0.07	0.00	0.09	3
INM-CM5-0	26.35	0.60	0.94	0.11	0.01	0.25	0.04	0.00	0.00	0.04	2
MRI-ESM2-0	79.22	14.21	0.44	0.32	0.24	0.11	0.07	0.15	0.01	0.23	4
CMCC-ESM2	89.83	32.64	0.60	0.36	0.55	0.16	0.08	0.36	0.01	0.44	5
Ideal values	15.71	0.6	0.99	0.06	0.01	0.26					
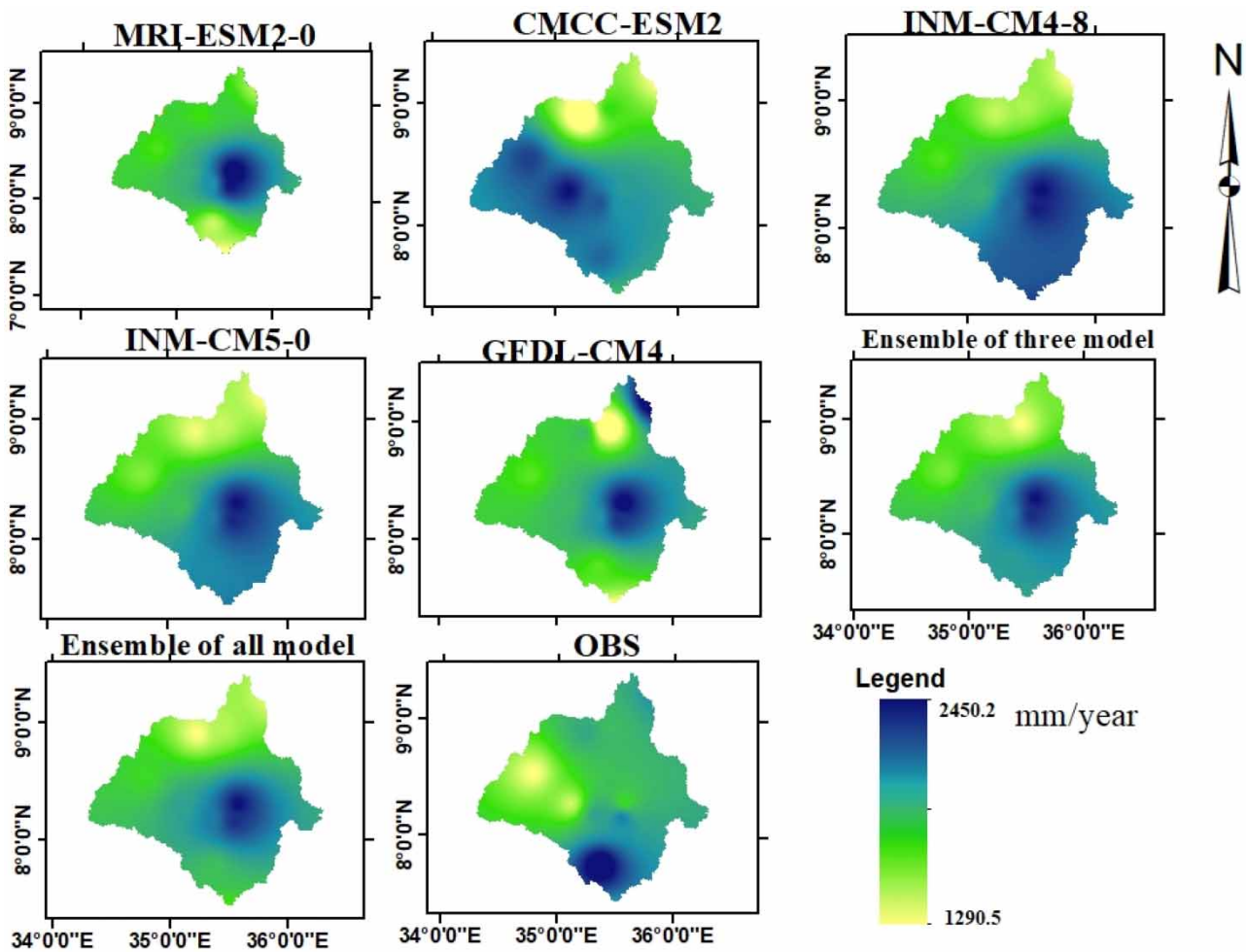
Figure 3 | Spatial distribution of the GCM and observed average annual precipitation over the Baro River Basin of historical simulation (1985–2014).

basin shows, the ensemble of the three models fits the observed precipitation better than the individual and ensemble of all models.

On a monthly basis, some models have underestimated precipitation at some months and overestimated some others. For example, the GFDL-CM4 was underestimated in all months except May, July August, and September whereas INM-CM4-8 was overestimated in all months except May, June, and July. The three models GFDL-CM4, INM-CM5-0, and INM-CM4-8 were unimodal, while the MRI-ESM2-0 and CMCC-ESM2 are bimodal over the basin as shown (Figure 4). However, the Baro River Basin is characterized by unimodal rainfall at all stations. Therefore, GCMs with unimodal precipitation are selected as the best representative GCMs in the study area.

The percentage bias for the ensembled three models is 0.55 and the percentage bias of all model ensemble and first ranked models are 9.701 and −5.53, respectively. This shows the performance of the three-model ensemble is superior to the ensemble of all models and the first ranked model GFDL-CM4.

The findings of GCMs performance evaluation in the Baro Akobo River basin show that CMIP6 GCMs are suitable to simulate the precipitation adequately. However, the selection of specific climate models for a specific region is subjective based on the factors considered and techniques used for evaluation. This is consistent with the study report by Almazroui *et al.* (2020) who reported CMIP6 GCMs are able to simulate the East African major climate variables. Similar findings of best performing models are reported in different parts of Africa. For example, a study by Ongoma *et al.* (2017) found GFDL-CM4 to be the best performing and first ranked model for annual precipitation simulation from the 15 GCMs evaluated in Uganda. On the other
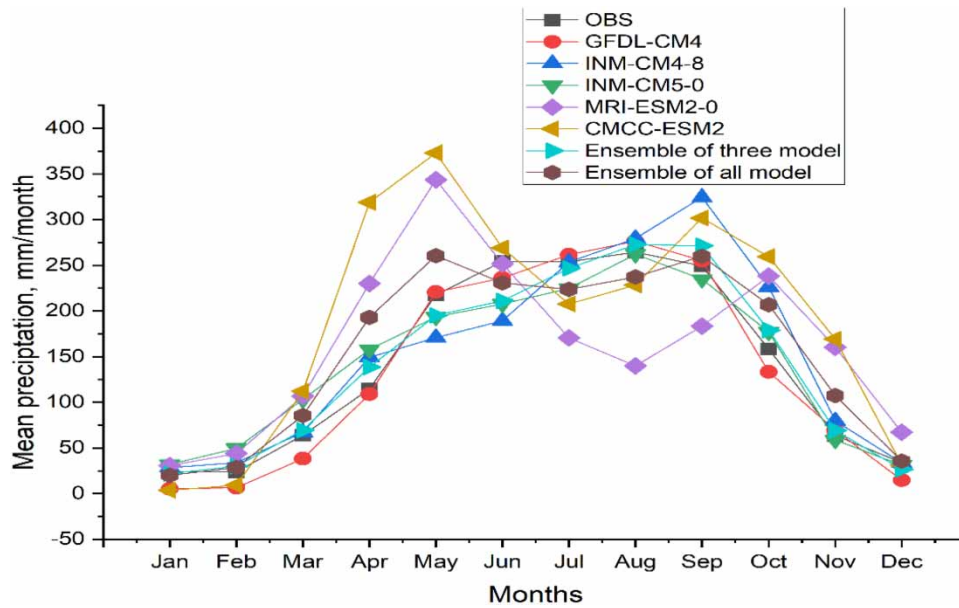
Figure 4 | Comparison of average monthly precipitation observed with the GCMs and their ensemble for historical simulation (1985–2014).

hand, Shiru & Chung (2021) reported INM-CM5-0 and INM-CM4-8 were ranked 11th and last from the 13 GCMs evaluated in Nigeria. The over/under estimation of mean monthly precipitation by some models reported in this study is also reported by Babaousmail *et al.* (2021) over North Africa. According to a study conducted by Babaousmail *et al.* (2021), the CMIP6 models effectively replicate the average annual climatic conditions during both dry and wet months. The findings of this study demonstrate that the CMIP6 models successfully replicate the mean monthly precipitation, with the top three ranked models performing particularly well. Nevertheless, a few models indicate a minor overestimation or underestimation for certain months. The study also reported adequate simulation of the mean ensemble than the individual models.

The variations in the spatial distribution of mean annual precipitation reported by the GCMs in Baro Akobo revealed that all models are not equally worth for specific locations and topographies. For example, the study by Dibaba *et al.* (2019) reported a varying spatial simulation of the climate models in the Finchaa and Didessa catchments. Especially, climate uncertainties in precipitation simulation increase in mountain regions. However, the mean ensemble of three models adequately estimated precipitation across the entire domain. However, the overall linear distribution over the basin shows the ensemble of the three models fits the observed precipitation better than the individual and ensemble of all models.

3.2. Performance of GCM for maximum temperature

The performance metrics for maximum temperature calculated for all GCMs and the ranking of GCMs derived using CP are presented in Table 4. The highest model ranking is CMCC-ESM2, MRI-ESM2-0, and INM-CM5-0, respectively. The least

Table 4 | GCM performances metrics and ranking of maximum temperature

GCM	Performance matrix			Normalized matrix			Normalized weighted matrix			Sum	Rank
	RMSE	PBIAS	R^2	RMSE	PBIAS	R^2	RMSE	PBIAS	R^2		
CMCC-ESM2	1.19	0.50	0.75	0.12	0.04	0.17	0.001	0.00	0.00	0.001	1
GFDL-CM4	2.30	8.11	0.96	0.22	0.59	0.22	0.023	0.44	0.00	0.461	5
INM-CM4-8	1.13	3.26	0.91	0.11	0.24	0.20	0.000	0.16	0.00	0.160	4
INM-CM5-0	2.51	0.94	0.92	0.25	0.07	0.21	0.027	0.03	0.00	0.054	3
MRI-ESM2-0	1.97	0.99	0.90	0.19	0.07	0.20	0.017	0.03	0.00	0.046	2
Ideal values	1.13	0.5	0.96	0.11	0.04	0.22					

ranked GCM for maximum temperature using the CP method was GFDL-CM4. For maximum temperature, the entropy method assigns weights of 0.202, 0.79, and 0.006 to the individual criteria RMSE, PBIAS, and R^2, respectively.

GFDL-CM4-8 underestimated the maximum temperature in all months and contains a large percentage bias (-8.11%) compared to other GCMs. CMCC-ESM2 overestimates the maximum temperature in all months except December, January, February, and May. The ensemble of all GCM's performance is weaker than the ensemble of the top three models because two models GFDL-CM4 and INM-CM4-8 have shown underestimation and are weak in simulating maximum temperature comparatively (Figure 5). This implies the average of all models including the better ranked model and least ranked model is not accurate when compared with an average of better ranked model and individual model. Similar results are reported by previous studies in different parts. Alaminie *et al.* (2021) found that MRI-ESM2-0 has shown the highest performance rank for maximum temperature from the 8 GCM evaluated with observed satellite data over the Upper Blue Nile Basin. Another study by Shiru & Chung (2021) reported that INM-CM5-0 was ranked fifth among the 13 GCMs evaluated over Nigeria for maximum temperature.

The spatial distribution of the historical (1985–2014) mean annual maximum temperature over the Baro River is shown in Figure 6. All GCMs and their ensemble overestimated maximum temperature around the western or outlet of the basin and all GCMs models underestimated temperatures around the eastern, northern, and southern parts of the basin. The ensemble of three models simulated the observed temperature better than all the other models.

3.3. Performance of GCM for minimum temperature

The performance metrics for minimum temperature calculated for all GCMs and the ranking of GCMs derived using CP are presented in Table 5. For minimum temperature, the entropy method assigns weights of 0.52, 0.41, and 0.063 to the individual criteria RMSE, PBIAS, and R^2, respectively. The top three ranking models are GFDL-CM4, INM-CM4-8, and INM-CM5-0, respectively.

The three models GFDL-CM4, CMCC-ESM2, and MRI-ESM2-0 overestimate minimum temperature in all months (Figure 7). Both the INM-CM4-8 and INM-CM5-0 models overestimate minimum temperature in all months except December, January, and February. The results are consistent with previous study reports. For example, Mengistu *et al.*(2021) pointed out that raw RCMs and their ensembles have shown an overestimation of the observed minimum temperature over most of
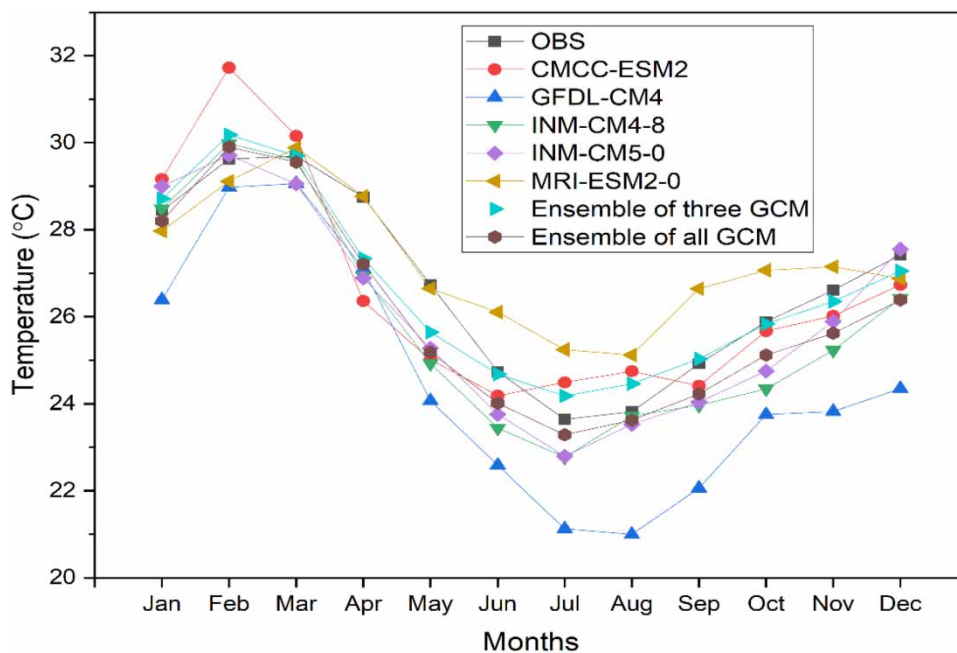

Figure 5 | Comparison of average monthly maximum temperature observed with five GCMs and ensemble model of historical simulation (1985–2014).
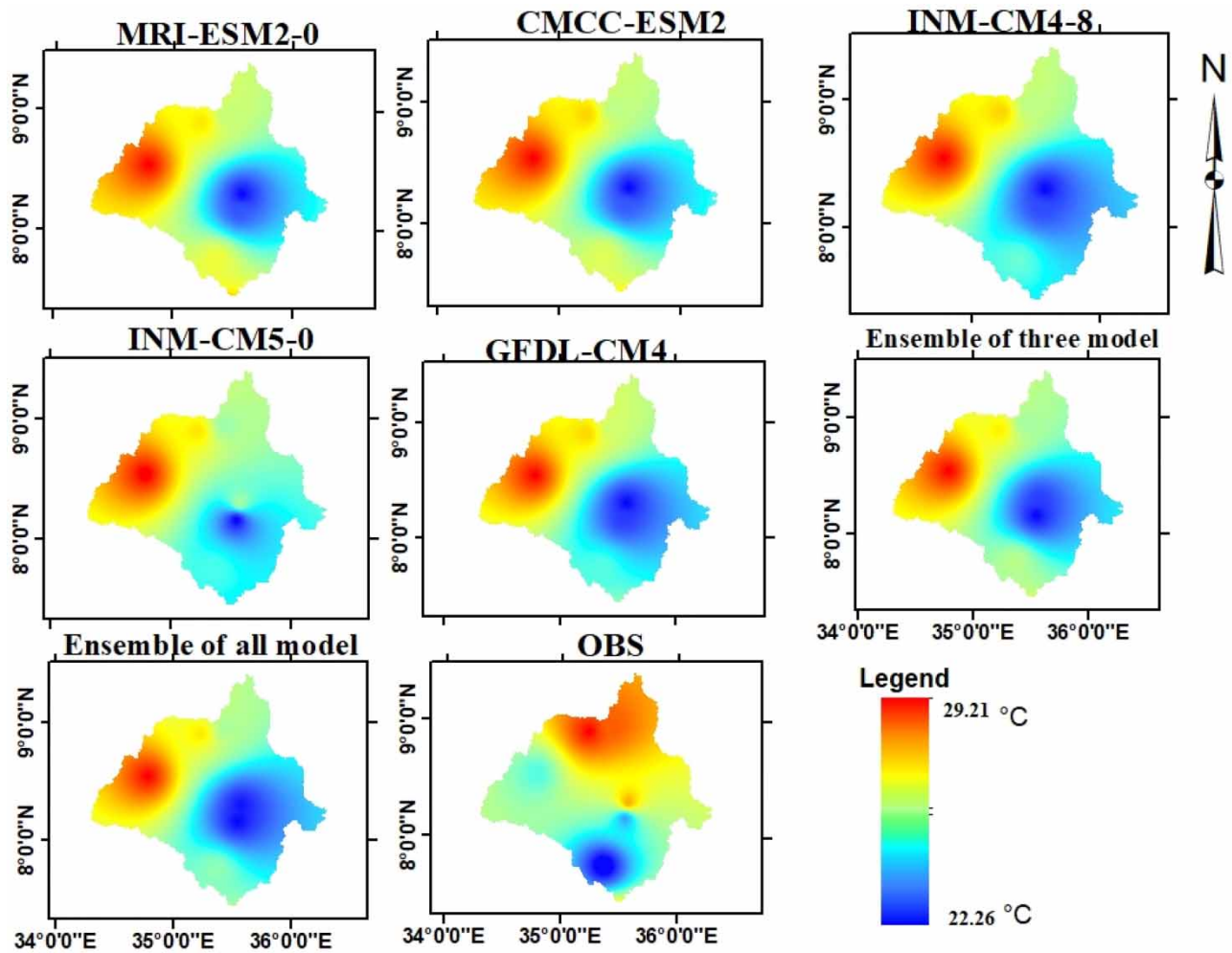
Figure 6 | Spatial distribution of GCMs and observed average maximum temperature over the Baro River Basin of historical simulation (1985–2014).

Table 5 | Performances metrics and ranking of minimum temperature GCMs

GCM	Performance matrix			Normalized matrix			Normalized weighted matrix			Sum	Rank
	RMSE	PBIAS	R^2	RMSE	PBIAS	R^2	RMSE	PBIAS	R^2		
CMCC-ESM2	5.58	42.1	0.82	0.25	0.31	0.21	0.08	0.09	0.001	0.171	5
GFDL-CM4	2.03	13.91	0.88	0.09	0.10	0.23	0.00	0.00	0.001	0.001	1
INM-CM4-8	3.5	19.34	0.56	0.16	0.14	0.14	0.04	0.02	0.006	0.057	2
INM-CM5-0	3.45	21.2	0.73	0.16	0.15	0.19	0.03	0.02	0.003	0.059	3
MRI-ESM2-0	5.34	40.45	0.91	0.24	0.30	0.23	0.08	0.08	0.000	0.159	4
Ideal values	2.03	13.91	0.91	0.09	0.10	0.23					

the stations in the Baro Akobo Basin. On the other hand, a study by Shiru & Chung (2021) found that INM-CM5-0 and INM-CM4-8 were ranked 3rd and 5th in simulating minimum temperature from 13 GCMs used for evaluation. In general, the CMIP6 GCMs tend to underestimate maximum temperatures while overestimating minimum temperatures when simulating the climate of the Baro Akobo River basin. Furthermore, the study found that overall biases were greater for minimum temperatures compared to maximum temperatures, on a monthly basis.
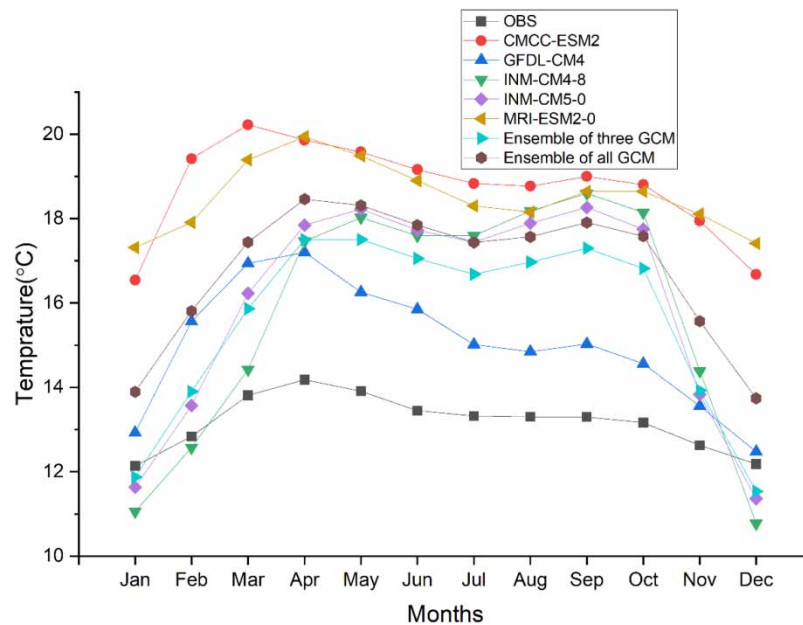
Figure 7 | Comparison of average monthly minimum temperature observed with five GCMs and ensemble model of the historical simulation (1985–2014).

The spatial distribution of the historical (1985–2014) mean annual minimum temperature over Baro River is shown in Figure 8. All GCMs and their ensemble overestimated the minimum temperature around the western or outlet of the parts of the basin. Overall, the ensemble of the three models has simulated the observed minimum temperature.

Overall, the study results show the importance of evaluating different GCMs into representative models and determining the most realistic ones for model aggregation into ensembles for climate projection to lessen the individual uncertainties linked to various GCMs. However, this choice does not necessarily guarantee that GCMs will be equally important for different climate variables. For example, GFDL-CM4, which performed well at precipitation, performed poorly for maximum temperature. Similarly, CMCC-ESM2 which is ranked 1st for maximum temperature showed a lower rank for precipitation and minimum temperature. Moreover, the best performing GCMs in one region or study area did not rank equally in other regions. To conduct a thorough assessment of climate models, it is essential to have a performance evaluation. According to Thorarinsdottir *et al.* (2020), climate model simulations must undergo an evaluation process by comparing the distributions of their outputs to the corresponding distributions of observational or reanalysis data products. Evaluating how well CMIP6 models simulate extreme climate events in the past can serve as a basis for generating dependable projections of future climate (Fan *et al.* 2020). According to Karim *et al.* (2020) efficient predictions of future climate changes depend on a thorough and accurate observation of past changes. Our study has examined how well each CMIP6 GCM performs in simulating the climate of the Baro Akobo river basin, particularly in relation to the distributions of daily observed climate variables.

3.4. Evaluation of bias-corrected precipitation and temperature

Raw GCMs outputs underestimate and overestimate the mean monthly precipitation as compared to the observed precipitation data. The statistical metrics such as PBIAS, RMSE, and R^2 showed a substantial difference between raw and bias-corrected GCMs output as compared to the observed long-term monthly precipitation data. The raw ensemble GCM simulations are heavily biased from observed data. For example, comparing the observed precipitation to the GCM output, the highest PBIAS (overestimation) was 30.06 and 26.83% for the Dembidollo and Bure stations, respectively. On the other hand, a large PBIAS (underestimation) was −20.85% for Masha and there is a small present bias in most stations (Table 6). The biases in the raw precipitation data were substantially reduced after applying a LS bias correction.

Table 7 compares the raw and bias-corrected monthly maximum and minimum temperature GCMs using PBIAS, RMSE, and R^2. The result showed that the raw output of the ensemble GCMs showed substantial biases compared to the observed data. For example, a large source of bias PBIAS (19.64%) and RMSE (4.46) was simulated for the Masha station. The
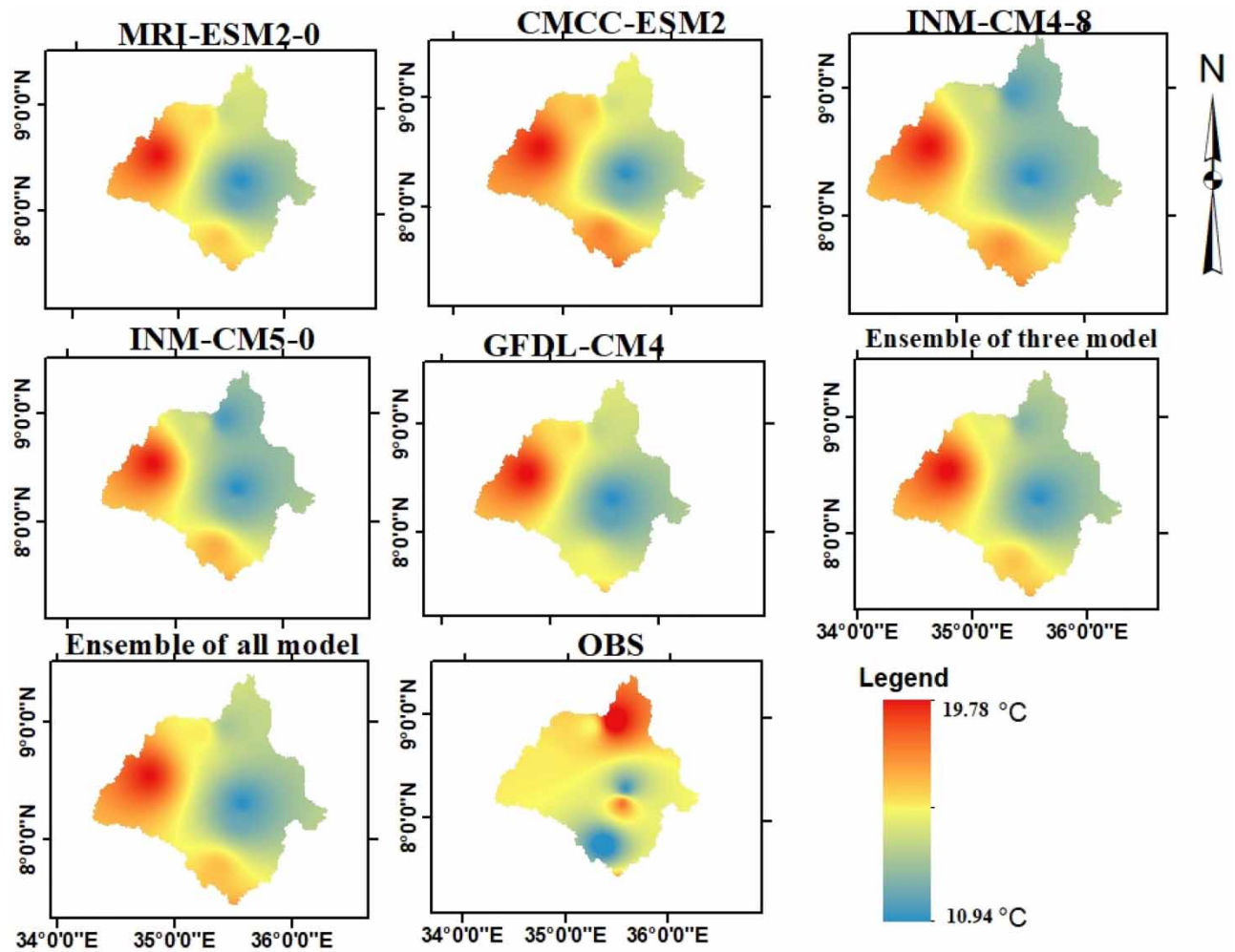
Figure 8 | Spatial distribution of the GCM and observed average minimum temperature over the Baro River Basin of historical simulation (1985–2014).

Table 6 | Statistical performance for raw and bias-corrected GCM precipitation

Station	Variable	RMSE	Before PBIAS	R^2	RMSE	Bias corrected PBIAS	R^2
Alem teferi	PCP	33.55	− 5.34	0.95	0.02	0.00	1.00
Bure	PCP	42.11	26.83	0.93	0.02	− 0.01	1.00
Dembidollo	PCP	51.01	30.06	0.86	0.03	− 0.01	1.00
Gimbi	PCP	45.05	− 7.44	0.96	0.01	0.00	1.00
Gore	PCP	23.39	− 2.26	0.95	0.00	0.00	1.00
Masha	PCP	47.16	− 20.85	0.92	0.01	0.00	1.00
Metu hospital	PCP	31.86	16.68	0.95	0.01	0.00	1.00
Mizen teferi	PCP	31.95	− 13.13	0.91	0.02	0.00	1.00
Tepi	PCP	31.13	8.93	0.89	0.01	0.00	1.00
Uka	PCP	23.64	− 0.35	0.95	0.02	0.00	1.00
Yubdo	PCP	10.26	− 2.93	0.96	0.01	− 0.01	1.00

Table 7 | Statistical performance measure of raw and bias-corrected GCM T$_{max}$ and T$_{min}$

Station	Variables	RMSE	Before PBIAS	R^2	Bias corrected RMSE	PBIAS	R^2
Alem teferi	T$_{max}$	0.71	− 7.79	0.84	0.00	0.00	1.00
	T$_{min}$	3.42	21.08	0.24	0.01	− 0.03	1.00
Dembidollo	T$_{max}$	2.51	9.73	0.93	0.00	0.00	1.00
	T$_{min}$	3.49	25.52	0.86	0.00	0.00	1.00
Gore	T$_{max}$	1.79	7.08	0.91	0.00	0.00	1.00
	T$_{min}$	2.71	8.43	0.09	0.02	− 0.03	1.00
Masha	T$_{max}$	4.46	19.64	0.79	0.00	0.00	1.00
	T$_{min}$	5.09	44.23	0.70	0.01	− 0.04	1.00
Metu	T$_{max}$	2.09	− 7.10	0.92	0.00	0.00	1.00
	T$_{min}$	3.87	32.25	0.91	0.02	− 0.06	1.00
Tepi	T$_{max}$	2.88	− 9.56	0.94	0.00	0.00	1.00
	T$_{min}$	1.30	6.13	0.89	0.00	0.00	1.00
Yubdo	T$_{max}$	2.30	− 7.21	0.91	0.00	0.00	1.00
	T$_{min}$	1.95	0.87	0.37	0.01	− 0.03	1.00

Note: T$_{max}$ and T$_{min}$ means maximum temperature and minimum temperature, respectively.

application of bias correction reduced the biases substantially at most of the stations. For example, the PBIAS of 19.64% and RMSE of 4.46 at the Masha station were removed after applying a bias correction, showing excellent agreement with the observed maximum temperature.

The results showed that the raw outputs from GCMs exhibited large biases for maximum and minimum temperatures. However, the biases were substantially reduced after applying DM bias correction. The improvement after bias correction particularly for PBIAS and RMSE was very good.

3.5. Quantifying the future climate projection

3.5.1. Precipitation projection

Bias-corrected mean annual and seasonal precipitation over the entire steady area for the future periods from 2031 to 2060 are presented in Table 8. The result shows that wet season precipitation is projected to increase by 9 mm (4.2%) and 27.2 mm (12.6%) under SSP2-4.5 and SSP5-8.5 scenarios, respectively. On the other hand, the projected annual precipitation was predicted to increase by 6.8 mm (6%) under the SSP2-4.5 and 23.63 mm (16.46%) under the SSP5-8.5 scenarios. The projected seasonal precipitation during the dry season shows increasing precipitation by 8 mm (19.15%) and 18 mm (44.4%) under the SSP2-4.5 and SSP5-8.5, respectively. Similar studies have reported an increasing trend of seasonal and annual precipitation in the future period (Ongoma *et al.* 2017; NAP 2019; Alaminie *et al.* 2021). Mekonnen & Disse's (2018) reported an increasing trend of precipitation, and temperature over the Upper Blue Nile River Basin using the ensemble mean of five GCMs.

Table 8 | Changes in mean annual precipitation for the future (2031–2060) relative to the baseline period (1985–2014)

Mean GCMs precipitation		Annual		AMJJASO		NDJFM	
Scenarios	SSP2-4.5	SSP5-8.5	SSP2-4.5	SSP5-8.5	SSP2-4.5	SSP5-8.5	
Baseline	143.48	143.48	216.03	216.03	41.91	41.91	
2031–2060	152.08	167.10	225.04	243.21	49.95	60.54	
Change (mm)	8.6	23.62	9.0	27.2	8.03	18	
Change (%)	6	16.46	4.2	12.6	19.15	44.4	

Similarly, a recent study by Alaminie *et al.* (2021) in the Upper Blue Nile River Basin reported an increasing precipitation trend under four SSP scenarios.

The projected monthly precipitation shows consistent directions and magnitude of change between SSP2-4.5 and SSP5-8.5 scenarios except for the month of July. The average monthly projected precipitation was increased under SSP2-4.5 scenarios except for July. The projected precipitation in SSP5-8.5 is greater than in the SSP2-4.5 scenarios. Ongoma *et al.* (2017) reported similar trends of precipitation projection in East Africa, stating the increase in precipitation under SSP5-8.5 are greater than under SSP2-4.5 scenarios. A similar study by Alaminie *et al.* (2021) found precipitation projected under SSP5-8.5 are greater than SSP2-4.5 in all months except July over the Upper Blue Nile basin. Almazroui *et al.* (2020) over North East Africa also reported increasing precipitation in SSP5-8.5, but SSP2-4.5 have no uniform trend of precipitation. Alternatively, the study conducted by Gebresellase *et al.* (2022) on the Awash basin projected that future precipitation and temperature changes will result in increased precipitation intensities, more wet days, and longer dry spells, primarily due to a significant rise in temperature. Likewise, this study demonstrated that the projected precipitation will increase in the future under both SSPs (SSP2-4.5 and SSP5-8.5). In general, the study indicates that there will be heightened future changes in the basin's climate, specifically with regard to increased precipitation and temperature. Precipitation increases have the potential to increase water availability, which will benefit water resources. However, this is not true always as reported by Dibaba *et al.* (2020). According to Dibaba *et al.* (2020), regardless of the increasing or decreasing precipitation, the availability of water is highly affected by the temperature change and the associated evapotranspiration demands. On the other hand, if the predicted precipitation increases, it could have a number of consequences for the environment and human society. Increased precipitation can lead to more frequent and intense flooding events, particularly in areas that are already prone to flooding. This could have negative consequences such as infrastructure damage, property loss, crop damage, and even death. While increased precipitation can be beneficial to agriculture and water resources, it can also cause soil erosion and water pollution. Heavy rain has the potential to wash away topsoil and transport pollutants from agricultural and urban areas, affecting waterways and jeopardizing water quality.

The spatial distribution of the precipitation under both (SSP2-4.5 and SSP5-8.5) climate projection scenarios is shown in Figure 9. The highest increase in annual precipitation is projected around the South of the basin and moderate around the North, under both SSP2-4.5 and SSP5-8.5 throughout the study projection considered compared with the historical period. The lowest precipitation in both SSPs is projected to the West, Northwest, and center of the basin. The spatial distribution of precipitation shows that the precipitation varies with the topography of the area. The higher elevation around the Masha receives the highest, and the lower elevation around the outlet receives less precipitation. This finding is in line with the study of NMA (2007). According to NMA (2007), Ethiopia's rainfall is influenced by several weather systems, including the Subtropical Jet (STJ), Intertropical Convergence Zone (ITCZ), Red Sea Convergence Zone (RSCZ), Tropical Easterly Jet (TEJ), and Somali Jet. These systems collectively contribute to the precipitation patterns observed in Ethiopia. The variation in rainfall amount and distribution, both across the country as a whole and within the specific study area, can be attributed to the factors of rate, location, direction, and variability of the aforementioned weather systems. These elements collectively influence the patterns of precipitation observed in the region.

3.5.2. Maximum temperature (T_{max}) projection

The projected maximum temperature shows an increase in mean seasonal and annual temperature under SSP2-4.5 and SSP5-8.5 scenarios. The mean annual maximum temperature is projected to increase by 1.43 and 1.81 °C under SSP2-4.5 and SSP5-8.5 scenarios, respectively, compared with baseline (historical). The projected average maximum temperature predicted for the wet season was slightly higher than for the dry season. The projected maximum temperature during the wet season from April to October increases by 1.67 and 2.17 °C under SSP2-4.5 and SSP5-8.5 scenarios, respectively. On the other hand, the projected average maximum temperature during the dry season from November to March increases by 1.09 and 1.3 °C under SSP2-4.5 and SSP5-8.5 scenarios, respectively (Table 9).

The simulated maximum temperature shows a consistent increase in all months under both SSP2-4.5 and SSP5-8.5 scenarios. The monthly maximum temperature increases in SSP2-4.5 range from 0.71 to 2.06 °C with a maximum increase in June, and the maximum temperature increase in SSP5-8.5 range from 0.92 to 2.65 °C, with a maximum increase in June. Overall, the increase in temperature reported in this study is consistent with the continuous increase in warming observed during the 21st century in the North Eastern Africa (Almazroui *et al.* 2020; Fan *et al.* 2020). According to Almazroui *et al.* (2020), temperature is projected to increase by 1.3 and 1.7 °C under SSP2-4.5 and SSP5-8.5, respectively. The temperature projections are

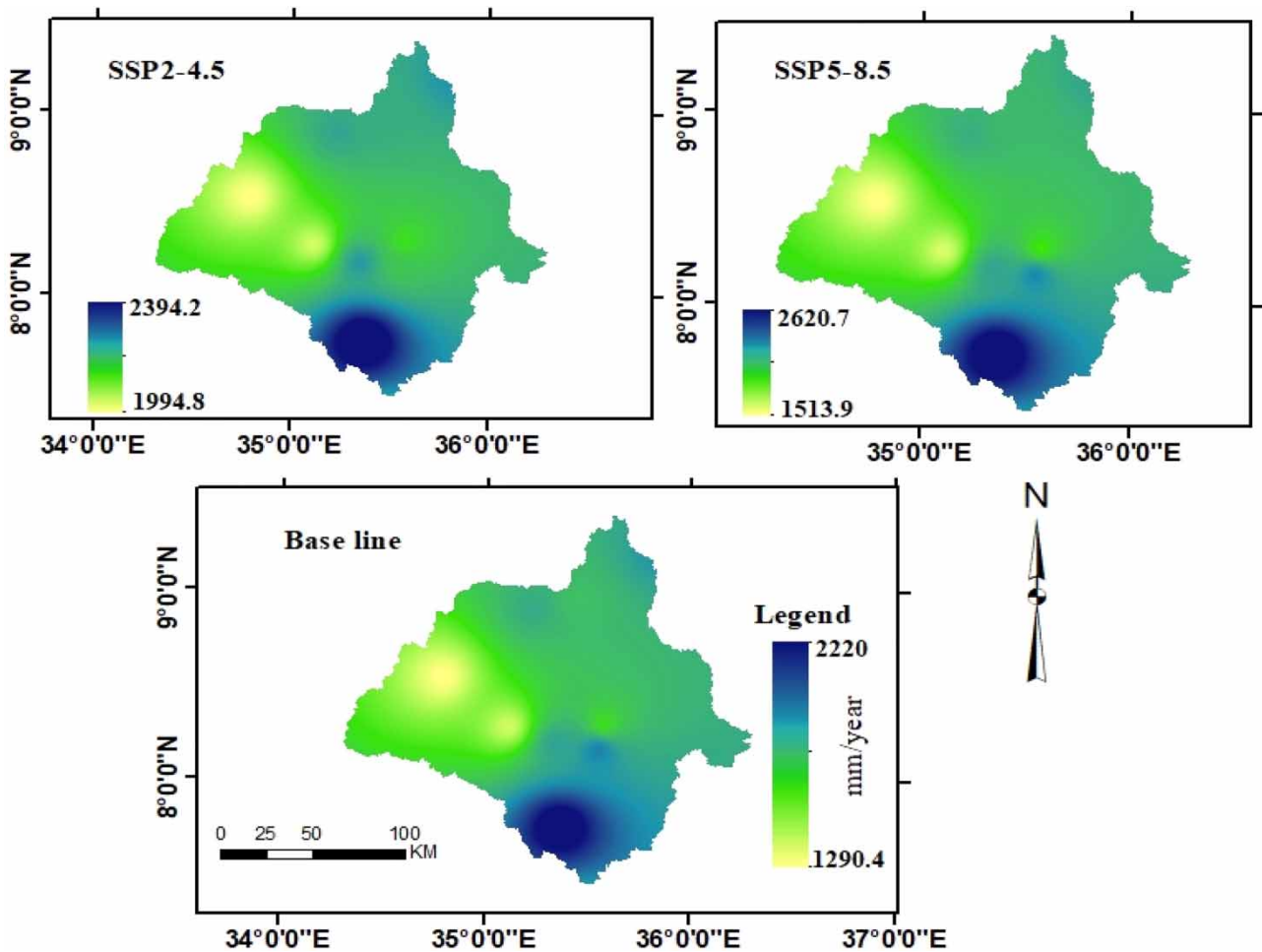**Figure 9** | Spatial distribution of annual precipitation (2031–2060).

Table 9 | Mean average seasonal and annual change of T$_{max}$ (2031–2060)

Mean T$_{max}$ (°C)		Annual		AMJJASO		NDJFM	
Scenarios	SSP2-4.5	SSP5-8.5	SSP2-4.5	SSP5-8.5	SSP2-4.5	SSP5-8.5	
Baseline	26.69	26.69	25.5	25.5	28.36	28.36	
2031–2060	28.12	28.5	27.17	27.67	29.45	29.66	
Change (°C)	1.43	1.81	1.67	2.17	1.09	1.3	

Note: T$_{max}$ denotes maximum temperature.

also in line with the previous studies in different parts of Ethiopia (NAP 2019; Getahun *et al.* 2020; Alaminie *et al.* 2021). For example, Alaminie *et al.* (2021) reported that the mean annual maximum temperature is projected to increase in the Upper Blue Nile basin by 1.3 and 1.5 °C under SSP2-4.5 and SSP5-8.5 scenarios, respectively, for near-term (2031–2060) period. Getachew *et al.* (2021) reported an increase in maximum temperatures by 1.38–3.59 °C by the 2080s in the Lake Tana sub-basin of Ethiopia under the RCP4.5 radiative forcing scenario. Rising temperatures have several significant implications. For example, the overall rise in temperature is attributed to these changes in precipitation patterns (Getachew *et al.* 2021). According to the study by Gurara *et al.* (2022), projected changes in future precipitation and temperature lead to increased precipitation intensities, more wet days, and longer dry spells in the Awash basin. The significant rise in temperature is

attributed to these changes. As temperatures rise, the atmosphere may change, changing rainfall patterns and causing more intense rainfall events to occur. It should be noted that the specific consequences of rising temperatures can vary depending on regional and local factors. The rise in temperature could also result in increased evapotranspiration demand which reduces the availability of water in the soil according to Dibaba *et al.* (2020).

The spatial distribution of maximum temperature under the SSP2-4.5 and SSP5-8.5 climate scenarios is shown in Figure 10. The annual average maximum temperature (2031–2060) shows that the highest increase is projected around the North and moderate around central, under both (SSP2-4.5 and SSP5-8.5) throughout the period considered compared with baseline (historical period). The lowest maximum temperature under both SSPs is projected around the South of the basin. The lower elevation around Mizen Tafari is highly warmer and the higher elevation around Masha is low warmest under both SSP2-4.5 and SSP5-8.5.

3.5.3. Minimum temperature (T_{min}) projection

Like maximum temperature, a projected minimum temperature show increases in seasonal and annual average temperature under SSP2-4.5 and SSP5-8.5 scenarios. The annual average minimum temperature is projected to increase by 1.96 and 3.11 °C under SSP2-4.5 and SSP5-8.5 scenarios, respectively. The projected average maximum temperature of the wet season was slightly greater than the dry season. The projected minimum temperature during the wet season from April to October increases by 2.32 and 3.62 °C under SSP2-4.5 and SSP5-8.5 scenarios, respectively. On the other hand, the projected average
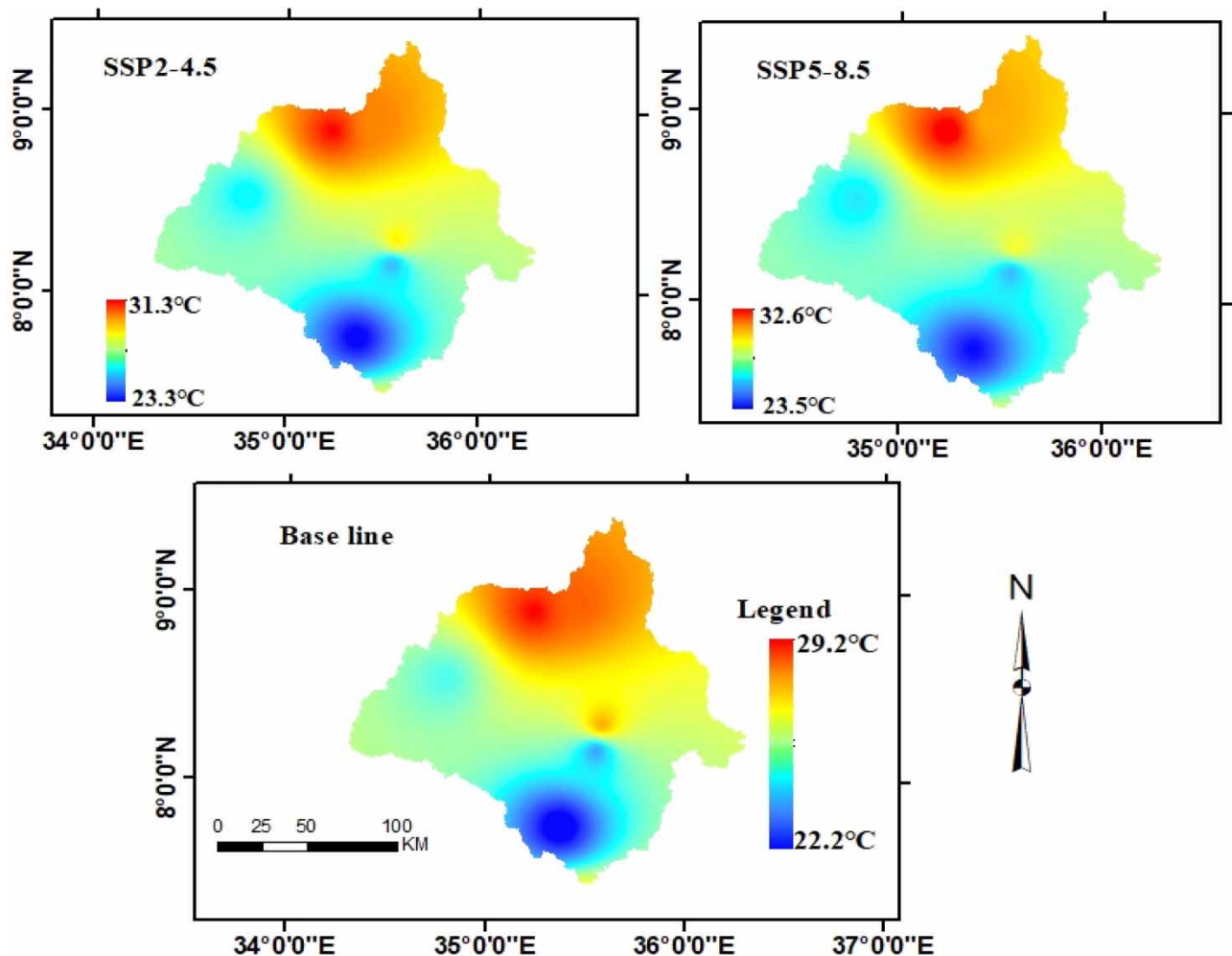

Figure 10 | Spatial distribution of maximum temperature (2031–2060).

minimum temperature during the dry season from November to March increases by 1.45 and 2.4 °C under SSP2-4.5 and SSP5-8.5 scenarios, respectively (Table 10).

The simulated minimum temperature shows a consistent increase in all months under both SSP2-4.5 and SSP5-8.5 scenarios compared with the baseline (historical period). The monthly minimum temperature increases under SSP2-4.5 is between 0.67 and 2.81 °C with the maximum increase in September, while minimum temperature increases under SSP5-8.5 range from 1.04 to 4.4 °C with the maximum increase in September. The simulated minimum temperature shows an increasing direction of change between SSP2-4.5 and SSP 5-8.5 scenarios in all months. An increase in minimum temperature is larger than the increase in maximum temperature projected under both SSP2-4.5 and SSP5-8.5 scenarios.

The results are consistent with previous studies. For example, a study by Getahun et al. (2020) indicated that the increase in minimum temperature for all GCMs was generally higher than the maximum temperature increase for both the 2021–2051 and 2071–2100 periods in the Melka Kunture sub-basin of the Awash basin, Ethiopia. Overall, increasing trends in temperature were reported by recent studies in North East Africa (Almazroui et al. 2020). This is in line with the recent IPCC's sixth assessment.

The spatial distribution of the minimum temperature under both (SSP2-4.5 and SSP5-8.5) scenarios is shown in Figure 11. The annual average minimum temperature (2031–2060) shows the highest increase around the North under both (SSP2-4.5 and SSP5-8.5) and the lowest minimum temperature under SSP2-4.5 is projected around the South and center of the basin compared with baseline (historical period). The lower elevation around Mizen Tafari is warmest than the higher elevation around Masha under both SSP2-4.5 and SSP5-8.5. This indicates that temperature varies according to the topography of the study area. The temperature condition demonstrates an inverse relationship with altitude (Gurara et al. 2022). In regions of low altitude, high temperatures prevail, whereas areas at higher altitudes experience the lowest temperatures.

3.5.4. Implication of climate change

The projected rise in temperatures and the anticipated fluctuations in precipitation will impact the hydrological cycle, thereby influencing future planning and development of the watershed. Agriculture plays a vital role as the backbone of the country's economy, and any fluctuations in productivity directly influence the growth of the Gross Domestic Product (GDP) (Addisu et al. 2015). Consequently, any alterations in the quantity and distribution of rainfall and temperature would pose a severe threat to agricultural productivity. These changes would have immediate implications for food production and security at a national level. Warmer minimum temperatures can extend growing seasons in these areas, allowing crops to grow for longer periods of time and potentially increasing agricultural productivity (Moges & Bhat 2021). While longer growing seasons can be beneficial, rising minimum temperatures can cause crop heat stress, lower yields, altered pollination patterns, and increased pest and disease pressure, posing challenges to agricultural production and food security. The increase in temperature not only impacts crop production but also has a profound effect on the growth and production patterns of livestock. According to Garnett (2009), as temperatures rise, livestock production faces detrimental consequences including intensified competition for natural resources, diminished feed quality and quantity, loss of biodiversity, and the additional challenge of increasing demands for livestock products.

The dynamic alterations in future rainfall, as stated in the IPCC's fifth assessment report (IPCC 2013), are largely attributable to the rise in global surface temperature induced by human activities. It is highly certain that in a considerably warmer world, changes in average precipitation will not occur uniformly. Certain regions will witness increases, while others may experience decreases or relatively minor alterations in precipitation patterns. According to Moges & Bhat (2021), even slight changes in the amount, distribution, and trends of rainfall can have a direct and substantial impact on agricultural

Table 10 | Mean average seasonal and annual change of T_{min} (2031–2060)

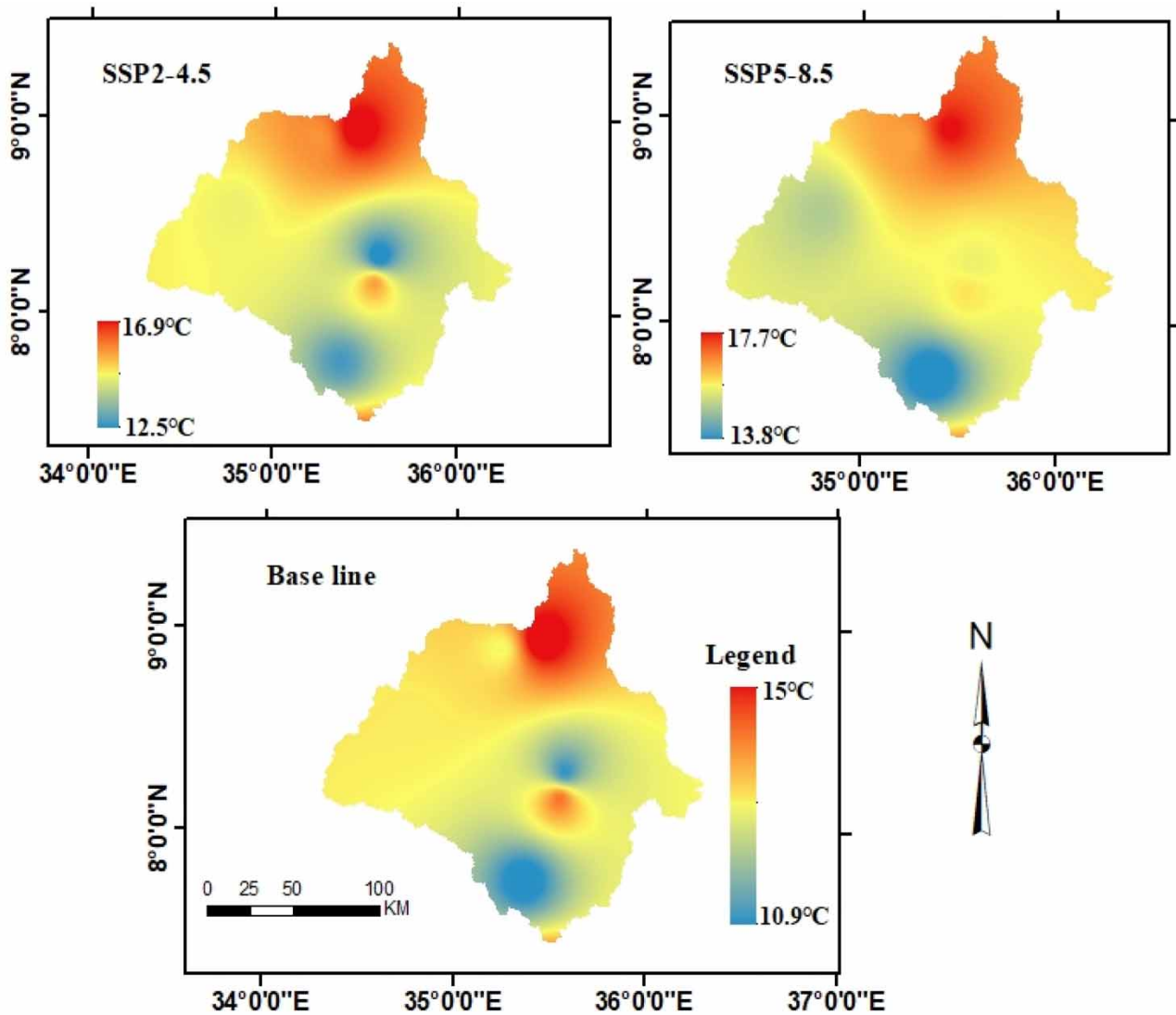| Average T_{min} (°C)	Annual			AMJJASO		NDJFM
Scenarios	SSP2-4.5	SSP5-8.5	SSP2-4.5	SSP5-8.5	SSP2-4.5	SSP5-8.5
Baseline	13.18	13.18	13.52	13.52	12.71	12.71
2031–2060	15.14	16.29	15.84	17.14	14.17	15.11
Change (°C)	1.96	3.11	2.32	3.62	1.45	2.4

Note: T_{min} denotes minimum temperature.

Figure 11 | Spatial distribution of minimum temperature (2031–2060).

production. Consequently, these variations significantly affect the lives of rural smallholder farmers who heavily rely on agriculture as their primary source of income. As stated by Fiwa *et al.* (2014), when excessive rainfall occurs without proper soil conservation structures in place, it results in a heightened rate of surface runoff and soil erosion. This, in turn, leads to the depletion of fertile topsoil in high slope areas and the accumulation of sedimentation in low slope areas. Flooding causes the inundation of agricultural fields, leading to the destruction of crops. Additionally, it can have a significant impact on the quality of grazing lands and irrigation facilities in the downstream watershed (Maharjan & Joshi 2013). The results of this study provide valuable insights into the spatial variations and temporal trends of rainfall and temperature. This information is crucial for effective water resource management and making informed decisions regarding farming practices.

4. CONCLUSIONS

This paper has evaluated the performance of five GCMs, which are part of CMIP6, to quantify the future precipitation and temperature changes under different scenarios. The performance evaluation of the individual GCMs and ensemble of the GCMs was held based on multi-criteria like mean annual spatial simulation, monthly analysis, CP and the combination of statistical metrics (PBIAS, RMSE, and R^2). The method of Entropy weighting was selected for the allocation of weights to

evaluate the dispersion of values. Three GCMs (GFDL-CM4, INM-CM5-0, and INM-CM4-8) outperformed precipitation simulations and two models (CMCC-ESM2 and MRI-ESM2) simulated precipitation poorly compared to the observed data (1985–2014). CMCC-ESM2, MRI-ESM2, and INM-CM5-0 are the top three models for maximum temperature simulation, whereas INM-CM5-0, and GFL-CM4, INM-CM5, and INM-CM4-8 are the top three models for minimum temperature simulation. The statistical performance evaluations for both precipitation and temperature show that the ensemble of three models outperforms both the individual and ensemble of all GCMs. The combination of statistical metrics, spatial and seasonal and annual climatology in the evaluation of CMIP6 over the Baro Akobo River basin showed that CMIP6 GCMs can be used for climate projections.

GCMs bias correction was processed using LS for precipitation and DM for temperature using the CMhyhd tool. For the climate change projections, the ensemble of the three models was bias-corrected to reduce the uncertainties associated with the individual GCMs. Annual and seasonal projected rainfall show an increasing trend under both SSP2-4.5 and SSP5-8.5 in the coming period (2031–2060) with reference to a baseline period (1985–2014). The projection of both maximum and minimum temperature shows an increasing trend under both SSPs, but the projected temperature under SSP5-8.5 is slightly greater than the projected temperature under SSP2-4.5. The increasing temperature may cause an increase in evapotranspiration and potential evapotranspiration, which in turn causes a reduction in soil water availability which could be a problem for subsistence agriculture. Overall, the changes in precipitation and increase in temperature will intensify under different climate change scenarios in the Baro Akobo River basin. In this regard, it is important to evaluate the climate change impacts which could help to understand the current and future change impacts. This could help to respond to what should happen that help to evaluate management/adaptations to compensate for the change impacts.

For future investigations in the basin, it is crucial to consider the evaluation of CMIP6 in simulating the precipitation extremes in order to evaluate the potential impacts of climate change on flooding and drought. In this study, the scenarios used for the projection of climate change are limited to two (SSP2-4.5 and SSP5-8.5). Therefore, similar studies should encompass a broad range of updated future forcing pathways, including both the middle to upper range and the lower end, to provide a comprehensive understanding for future research. With the set of criteria developed based on a nominal resolution of 100 km and GCMs with the first member (r1i1plf1), only 5GCMs are used. If the criteria change, there is a possibility to get many more GCMs. Moreover, this study used only five GCMs and with a set of criteria developed based on a nominal resolution of 100 km.

In this study, the ensemble of three models outperforms the ensemble of all models in the Baro River Basin. Overall, the best model for one climate variable (precipitation) may not be representative of the other variable (temperature), so it is important to evaluate the performance of both precipitation and temperature. The anticipated rise in precipitation levels has the potential to create a flood risk. Therefore, we suggest utilizing the average output from the highest-ranked models to examine the hydrological response to climate change. The result highlights the need for regional development and cooperation to promote strong climate-resilient management strategies and to counteract the rapid climate changes projected in the study area. In order to support decision makers, planners and stakeholders to devise appropriate basin management strategies, evaluating the potential impacts of climate change on the hydrology and water resources of the Baro Akobo basin will be the continuation of this study.

DATA AVAILABILITY STATEMENT

All relevant data are included in the paper or its Supplementary Information.

CONFLICT OF INTEREST

The authors declare there is no conflict.

REFERENCES

Addisu, S., Selassie, Y. G., Fissha, G. & Gedif, B. 2015 Time series trend analysis of temperature and rainfall in lake Tana Sub-basin, Ethiopia. *Environmental Systems Research* **4** (1). https://doi.org/10.1186/s40068-015-0051-0.

Afolayan, A., Ongoma, V. & Kooperman, G. J. 2021 Evaluation of CMIP6 models in simulating the statistics of extreme precipitation over Eastern Africa. *Atmospheric R* **254** (November 2020), 1–12. https://doi.org/10.1016/j.atmosres.2021.105509.

Alaminie, A. A., Tilahun, S. A., Legesse, S. A., Zimale, F. A., Jury, G. B. T. & Jury, M. R. 2021 Evaluation of past and future climate trends under CMIP6 scenarios for the UBNB (Abay), Ethiopia. *Water*. https://doi.org/10.3390/w13152110.

Almazroui, M., Saeed, F., Saeed, S., Nazrul Islam, M., Ismail, M., Klutse, N. A. B. & Siddiqui, M. H. 2020 Projected change in temperature and precipitation over Africa from CMIP6. *Earth Systems and Environment* **4** (3), 455–475. https://doi.org/10.1007/s41748-020-00161-x.

Anil, S., Manikanta, V. & Pallakury, A. R. 2021 Unravelling the influence of subjectivity on ranking of CMIP6 based climate models: A case study. *International Journal of Climatology* **41** (13), 5998–6016. https://doi.org/10.1002/joc.7164.

Babaousmail, H., Hou, R., Ayugi, B., Ojara, M., Ngoma, H., Karim, R., Rajasekar, A. & Ongoma, V. 2021 Evaluation of the performance of CMIP6 models in reproducing rainfall patterns over North Africa. *Atmosphere Article* **12**, 1–25. https://doi.org/10.3390/atmos12040475.

Bodian, A., Dezetter, A., Diop, L., Deme, A., Djaman, K. & Diop, A. 2018 Future climate change impacts on streamflows of and Gambia. *Hydrology*. https://doi.org/10.3390/hydrology5010021.

Chen, H., Sun, J., Lin, W. & Xu, H. 2020 Comparison of CMIP6 and CMIP5 models in simulating climate extremes. *Science Bulletin* **65**, 1415–1418. https://doi.org/10.1016/j.scib.2020.05.015.

Dibaba, W. T., Miegel, K. & Demissie, T. A. 2019 Evaluation of the CORDEX regional climate models performance in simulating climate conditions of two catchments in Upper Blue Nile Basin. *Dynamics of Atmospheres and Oceans* **87**, 101104. https://doi.org/10.1016/j.dynatmoce.2019.101104.

Dibaba, W. T., Demissie, T. A. & Miegel, K. 2020 Watershed hydrological response to combined land Use/Land cover and climate change in Highland Ethiopia: Finchaa Catchment. *Water*. https://doi.org/10.3390/w12061801.

Eyring, V., Bony, S., Meehl, G. A., Senior, C. A., Stevens, B., Stouffer, R. J., Taylor, K. E., Dynamique, D. M., Pierre, I., Laplace, S. & Ipsl, L. M. D. 2016 Overview of the Coupled Model Intercomparison Project phase 6 (CMIP6) experimental design and organization. *Geoscientific Model Development* 1937–1958. https://doi.org/10.5194/gmd-9-1937-2016.

Fan, X., Miao, C., Duan, Q., Shen, C. & Wu, Y. 2020 The performance of CMIP6 versus CMIP5 in simulating temperature extremes over the global land surface. *Journal of Geophysical Research: Atmospheres* **125** (18), 1–16. https://doi.org/10.1029/2020JD033031.

Fang, G. H., Yang, J., Chen, Y. N. & Zammit, C. 2015 Comparing bias correction methods in downscaling meteorological variables for a hydrologic impact study in an arid area in China. *Hydrology and Earth System Sciences* **19** (6), 2547–2559. https://doi.org/10.5194/hess-19-2547-2015.

Fiwa, L., Vanuytrecht, E., Wiyo, K. A. & Raes, D. 2014 Effect of rainfall variability on the length of the crop growing period over the past three decades in central Malawi. *Climate Research* **62** (1), 45–58. https://doi.org/10.3354/cr01263.

Flint, L. E. & Flint, A. L. 2012 Downscaling future climate scenarios to fine scales for hydrologic and ecological modeling and analysis. *Ecological Process* **1** (2), 1–15. https://doi.org/10.1186/2192-1709-1-2.

Garnett, T. 2009 Livestock-related greenhouse gas emissions: Impacts and options for policy makers. *Environmental Science and Policy* **12** (4), 491–503. https://doi.org/10.1016/j.envsci.2009.01.006.

Ge, F., Zhu, S., Luo, H., Zhi, X. & Wang, H. 2021 Future changes in precipitation extremes over Southeast Asia: Insights from CMIP6 multi-model ensemble. *Environmental Research Letters* **16**, 1–11. https://doi.org/10.1088/1748-9326/abd7ad.

Gebresellase, S. H., Wu, Z., Xu, H. & Muhammad, W. I. 2022 Evaluation and selection of CMIP6 climate models in Upper Awash Basin (UBA), Ethiopia: Evaluation and selection of CMIP6 climate models in Upper Awash Basin (UBA), Ethiopia. *Theoretical and Applied Climatology* **149** (3–4), 1521–1547. https://doi.org/10.1007/s00704-022-04056-x.

Getachew, B., Manjunatha, B. R. & Bhat, H. G. 2021 Modeling projected impacts of climate and land use/land cover changes on hydrological responses in the Lake Tana Basin, upper Blue Nile River Basin, Ethiopia. *Journal of Hydrology* **595** (January), 125974. https://doi.org/10.1016/j.jhydrol.2021.125974.

Getahun, Y. S., Li, M.-H. & Li, M.-H. 2020 Assessing impact of climate change on hydrology of Melka Kuntrie Subbasin, Ethiopia with Ar4 and Ar5 projections. *Water* **12**, 1–23. https://doi.org/10.3390/w12051308.

Gidden, M. J., Riahi, K., Smith, S. J., Fujimori, S., Luderer, G., Kriegler, E., Van Vuuren, D. P., Van Den Berg, M., Feng, L., Klein, D., Calvin, K., Doelman, J. C., Frank, S., Fricko, O., Harmsen, M., Hasegawa, T., Havlik, P., Hilaire, J., Hoesly, R. & Takahashi, K. 2019 Global emissions pathways under different socioeconomic scenarios for use in CMIP6: A dataset of harmonized emissions trajectories through the end of the century. *Geoscientific Model Development* **12** (4), 1443–1475. https://doi.org/10.5194/gmd-2018-266.

Gurara, M. A., Jilo, N. B., Tolche, A. D. & Kassa, A. K. 2022 Climate change projection using the statistical downscaling model in Modjo watershed, upper Awash River Basin, Ethiopia. *International Journal of Environmental Science and Technology* **19** (9), 8885–8898. https://doi.org/10.1007/s13762-021-03752-x.

IPCC. 2013 Intergovernmental panel on climate change. In: *Climate Change 2013: The Physical Science Basis. Contribution of Working Group I to the Fifth Assessment Report of the Intergovernmental Panel on Climate Change* (Stocker, T. F., Qin, D., Plattner, G.-K., Tignor, M., Allen, S. K., Boschung, J., Nauels, A., Xia, Y., Bex, V. & Midgley, P. M. eds). Cambridge University Press, Cambridge, United Kingdom and New York, NY, USA.

Jaagus, J. & Mändla, K. 2014 Climate change scenarios for Estonia based on climate models from the IPCC fourth assessment report. *Earth Sciences* 166–180. https://doi.org/10.3176/earth.2014.15.

Kadkhodazadeh, M., Anaraki, M. V., Morshed-Bozorgdel, A. & Farzin, S. 2022 A New methodology for reference evapotranspiration prediction and uncertainty analysis under climate change conditions based on machine learning, multi criteria decision making and Monte Carlo Methods. *Sustainability (Switzerland)* 14 (5). https://doi.org/10.3390/su14052601.

Karim, R., Tan, G., Ayugi, B. & Babaousmail, H. 2020 Evaluation of historical CMIP6 model simulations of seasonal mean temperature over Pakistan during 1970–2014. *Atmosphere*. https://doi.org/10.3390/atmos11091005.

Kebede, K. A., Moges, S. & Bernd, D. 2013 An assessment of temperature and precipitation change projections using a regional and a global climate model for the Baro-Akobo Basin, Nile Basin, Ethiopia. *Earth Science and Climatic Change*. https://doi.org/10.4172/2157-7617. 1000133.

Khan, M. S., Coulibaly, P. & Dibike, Y. 2006 Uncertainty analysis of statistical downscaling methods using Canadian Global Climate Model predictors. *Hydrological Processes* 20 (14), 3085–3104. https://doi.org/10.1002/hyp.6084.

Kim, Y. H., Min, S. K., Zhang, X., Sillmann, J. & Sandstad, M. 2020 Evaluation of the CMIP6 multi-model ensemble for climate extreme indices. *Weather and Climate Extremes* 29, 100269. https://doi.org/10.1016/j.wace.2020.100269.

Kumar, T. V. L., Vinodhkumar, B., Rao, K. K., Chowdary, J. S., Osuri, K. K. & Desamsetti, S. 2023 Insights from the bias-corrected simulations of CMIP6 in India's future climate. *Global and Planetary Change* 226, 104137. https://doi.org/10.1016/J.GLOPLACHA.2023.104137.

Luo, M., Liu, T., Meng, F., Duan, Y., Frankl, A., Bao, A. & De Maeyer, P. 2018 Comparing bias correction methods used in downscaling precipitation and temperature from regional climate models: A case study from the Kaidu River Basin in Western China. *Water* 10 (8). https://doi.org/10.3390/w10081046.

Maharjan, K. L. & Joshi, N. P. 2013 *Climate Change, Agriculture and Rural Livelihoods in Developing Countries*. Springer, Tokyo, Japan. https://doi.org/10.1007/978-4-431-54343-5.

Mekonnen, D. F. & Disse, M. 2018 Analyzing the future climate change of the Upper Blue Nile River basin using statistical downscaling techniques. *Hydrology and Earth System Sciences* 2391–2408. https://doi.org/10.5194/hess-22-2391-2018.

Melke, A. 2015 *Impact of Climate Change on Hydrological Responses of Gumara Catchment, in the Lake Tana Basin – Upper Blue Nile Basin of Ethiopia*. Addis Ababa University, Addis Ababa, Ethiopia.

Mengistu, D., Bewket, W., Dosio, A. & Panitz, H. 2020 Climate change impacts on water resources in the Upper Blue Nile (Abay) River Basin, Ethiopia. *Journal of Hydrology* 1–44. https://doi.org/10.1016/j.jhydrol.2020.125614.

Mengistu, A. G., Woldesenbet, T. & Yihun, T. D. 2021 *Evaluation of the Performance of Bias-Corrected CORDEX Regional Climate Models in Reproducing Baro – Akobo Basin Climate*. Springer, pp. 751–767. https://doi.org/10.1007/s00704-021-03552-w.

Moges, D. M. & Bhat, H. G. 2021 Climate change and its implications for rainfed agriculture in Ethiopia. *Journal of Water and Climate Change* 12 (4), 1229–1244. https://doi.org/10.2166/wcc.2020.058.

Muhammad, M. K. I., Nashwan, M. S., Shahid, S., Ismail, T. b., Song, Y. H. & Chung, E. S. 2019 Evaluation of empirical reference evapotranspiration models using compromise programming: A case study of Peninsular Malaysia. *Sustainability (Switzerland)* 11 (16). https://doi.org/10.3390/su11164267.

Muleta, T. N. 2021 Climate change scenario analysis for Baro - Akobo river basin, Southwestern Ethiopia. *Environmental Systems Research*. https://doi.org/10.1186/s40068-021-00225-5.

NAP 2019 *Ethiopia's Climate Resilient Green Economy National Adaptation Plan* (Issue May)..

Ngoma, H., Wen, W., Ayugi, B., Karim, R. & Ongoma, V. 2021 Evaluation of precipitation simulations in CMIP6 models over Uganda. *International Jornal of Climatology*. November 2020, 1–26. https://doi.org/10.1002/joc.7098.

NMA (2007). *Climate chaange National Adaptation Programme of Action (NAPA) of Ethiopia* (Issue June).

O'Neill, B. C., Kriegler, E., Riahi, K. & Ebi, K. L. 2014 *A new Scenario Framework for Climate Change Research : The Concept of Shared Socioeconomic Pathways*. Springer, pp. 387–400. https://doi.org/10.1007/s10584-013-0905-2.

O'Neill, B. C., Tebaldi, C., Vuuren, D. P. V., Eyring, V., Friedlingstein, P., Hurtt, G., Knutti, R., Kriegler, E., Lamarque, J., Lowe, J., Meehl, G. A. & Moss, R. 2016 The Scenario Model Intercomparison Project (ScenarioMIP) for CMIP6. *Geoscientific Model Development* 3461–3482. https://doi.org/10.5194/gmd-9-3461-2016.

Ongoma, V., Chen, H. & Gao, C. 2017 Projected changes in mean rainfall and temperature over East Africa based on CMIP5 models. *Royal Meteorological Society*. https://doi.org/10.1002/joc.5252.

Perez-Verdin, G., Monarrez-Gonzalez, J. C., Tecle, A. & Pompa-Garcia, M. 2018 Evaluating the multi-functionality of forest ecosystems in northern Mexico. *Forests* 9 (4), 1–14. https://doi.org/10.3390/f9040178.

Raju, K. S. & Kumar, D. N. 2020 Review of approaches for selection and ensembling of GCMS. *Journal of Water and Climate Change* 11 (3), 577–599. https://doi.org/10.2166/wcc.2020.128.

Rathjens, H., Bieger, K., Srinivasan, R. & Arnold, J. G. 2016 *CMhyd User Manual, Documentation for Preparing Simulated Climate Change Data for Hydrologic Impact Studies*. Available online: https://swat.tamu.edu/media/115265/bias_cor_man.pdf (accessed: August 20, 2022).

Roth, V., Lemann, T., Zeleke, G. & Teklay, A. 2018 Effects of climate change on water resources in the upper Blue Nile Basin of Ethiopia. *Heliyon* 1–28. https://doi.org/10.1016/j.heliyon.2018.e00771.

Salihu, A. C. 2018 *Climate Change Impact on Water Resources Availability in Gunia and Sudano-Sahelian Ecological Zones of Nigeria*. Federal University of Technology, Minna, Nigeria.

Shiferaw, H., Gebremedhin, A., Gebretsadkan, T. & Zenebe, A. 2018 Modelling hydrological response under climate change scenarios using SWAT model: The case of Ilala watershed, Northern Ethiopia. *Modeling Earth Systems and Environment* 4 (1), 437–449. https://doi.org/10.1007/s40808-018-0439-8.

Shiru, M. S. & Chung, E. S. 2021 *Performance Evaluation of CMIP6 Global Climate Models for Selecting Models for Climate Projection Over Nigeria*. Springer, pp. 599–615. https://doi.org/10.1007/s00704-021-03746-2.

Srivastava, A., Grotjahn, R. & Ullrich, P. A. 2020 Evaluation of historical CMIP6 model simulations of extreme precipitation over contiguous US regions. *Weather and Climate Extremes* 29, 100268. https://doi.org/10.1016/j.wace.2020.100268.

Sylla, M. B., Nikiema, P. M., Gibba, P., Kebe, I. & Klutse, N. A. B. 2016 Climate change over West Africa: recent trends and future projections Mouhamadou. In: *Adaptation to Climate Change and Variability in Rural West Africa*. Springer. https://doi.org/DOI: 10.1007/978-3-319-31499-0_3.

Taye, M. T., Dyer, E., Hirpa, F. A. & Charles, K. 2018 Climate change impact on water resources in the Awash basin, Ethiopia. *Water (Switzerland)* 10 (11), 1–16. https://doi.org/10.3390/w10111560..

Teutschbein, C. & Seibert, J. 2012 Bias correction of regional climate model simulations for hydrological climate-change impact studies: Review and evaluation of different methods. *Journal of Hydrology* s 456–457, 12–29. https://doi.org/10.1016/j.jhydrol.2012.05.052.

Thorarinsdottir, T. L., Sillmann, J., Haugen, M., Gissibl, N. & Sandstad, M. 2020 Evaluation of CMIP5 and CMIP6 simulations of historical surface air temperature extremes using proper evaluation methods. *Environmental Research Letters* 15 (12). https://doi.org/10.1088/1748-9326/abc778.

Tumsa, B. C. 2022 Performance assessment of six bias correction methods using observed and RCM data at upper Awash basin, Oromia, Ethiopia. *Journal of Water and Climate Change* 13 (2), 664–683. https://doi.org/10.2166/wcc.2021.181.

Worku, G., Teferi, E., Bantider, A., Dile, Y. T. & Taye, M. T. 2018 Evaluation of regional climate models performance in simulating rainfall climatology of Jemma Sub-basin, Upper Blue Nile Basin, Ethiopia. *Dynamics of Atmospheres and Oceans*. https://doi.org/10.1016/j.dynatmoce.2018.06.002.

Worku, G., Teferi, E., Bantider, A. & Dile, Y. T. 2019 Statistical bias correction of regional climate model simulations for climate change projection in the Jemma sub-basin, upper Blue Nile Basin of Ethiopia. *Theoretical and Applied Climatology* 139 (3–4), 1569–1588. https://doi.org/10.1007/s00704-019-03053-x.

Wu, Y., Miao, C., Sun, Y., AghaKouchak, A., Shen, C. & Fan, X. 2021 Global observations and CMIP6 simulations of compound extremes of monthly temperature and precipitation. *GeoHealth* 5, 1–13. https://doi.org/10.1029/2021GH000390.

Zeleny, M. 1973 *Compromise programming. Multiple criteria decision making*.

Zhang, X., Hua, L. & Jiang, D. 2021 Assessment of CMIP6 model performance for temperature and precipitation in Xinjiang, China. *Atmospheric and Oceanic Science Letters*. September, 1–8. https://doi.org/10.1016/j.aosl.2021.100128.

Zhou, B., Xu, Y. & Han, Z. 2021 CMIP6 evaluation and projection of temperature and precipitation over China CMIP6 evaluation and projection of temperature and precipitation over China. *Atmospheric Science* 38 (April). https://doi.org/10.1007/s00376-021-0351-4.

Zhu, Y., Tian, D. & Yan, F. 2020 Effectiveness of entropy weight method in decision-making. *Mathematical Problems in Engineering* 2020, 1–5. https://doi.org/10.1155/2020/3564835.